MNRAS 000, 1–16 (2018) Preprint 21 November 2018 Compiled using MNRAS LaTeX style file v3.0

The *Kepler* Smear Campaign I: An Asteroseismic Catalogue of Bright Red Giants

Benjamin J. S. Pope,[1,2,3★] Guy R. Davies,[4,5] Keith Hawkins,[6] Timothy R. White,[7,5] Allyson Bieryla,[8] David W. Latham,[8], Conny Aerts,[9,10,11] Suzanne Aigrain,[3] Victoria Antoci,[5] Timothy R. Bedding,[12,5] Dominic M. Bowman,[10] Ashley Chontos,[13] Gilbert A. Esquerdo,[8] Daniel Huber,[13,14,8] Paula Jofré,[15] Simon Murphy,[12,5] Timothy van Reeth,[12,5] Victor Silva Aguirre,[5] Amalie Stokholm,[5] Jie Yu[12,5]

[1] *Center for Cosmology and Particle Physics, Department of Physics, New York University, 726 Broadway, New York, NY 10003, USA*
[2] *NASA Sagan Fellow*
[3] *Oxford Astrophysics, Denys Wilkinson Building, University of Oxford, OX1 3RH, Oxford, UK*
[4] *School of Physics and Astronomy, University of Birmingham, Birmingham B15 2TT, UK*
[5] *Stellar Astrophysics Centre, Department of Physics and Astronomy, Aarhus University, Ny Munkegade 120, DK-8000 Aarhus C, Denmark*
[6] *Department of Astronomy, The University of Texas at Austin, 2515 Speedway Boulevard, Austin, TX 78712, USA*
[7] *Research School of Astronomy and Astrophysics, Mount Stromlo Observatory, The Australian National University, Canberra, ACT 2611, Australia*
[8] *Harvard-Smithsonian Center for Astrophysics, 60 Garden Street, Cambridge, MA 02138, USA*
[9] *Institute of Astronomy, KU Leuven, Celestijnenlaan 200D, B-3001 Leuven, Belgium*
[10] *Department of Astrophysics, IMAPP, Radboud University Nijmegen, P.O. Box 9010, 6500 GL Nijmegen, The Netherlands*
[11] *Kavli Institute for Theoretical Physics, University of California, Santa Barbara, CA 93106, USA*
[12] *Sydney Institute for Astronomy (SIfA), School of Physics, University of Sydney, NSW 2006, Australia*
[13] *Institute for Astronomy, University of Hawai'i, 2680 Woodlawn Drive, Honolulu, HI 96822, USA*
[14] *SETI Institute, 189 Bernardo Avenue, Mountain View, CA 94043, USA*
[15] *Núcleo de Astronomía, Facultad de Ingeniería y Ciencias, Universidad Diego Portales, Ejército 441, Santiago De, Chile*

Accepted XXX. Received YYY; in original form ZZZ

ABSTRACT

Here we present the first data release of the *Kepler* Smear Campaign, using collateral 'smear' data obtained by *Kepler* to reconstruct light curves of 102 stars too bright to have been otherwise targeted. We describe the pipeline developed to extract and calibrate these light curves, and show that we attain photometric precision comparable to stars analyzed by the standard pipeline in the nominal *Kepler* mission. In this Paper, we focus in particular on a subset of these consisting of 66 red giants for which we detect solar-like oscillations. All source code, light curves, TRES spectra, and asteroseismic and stellar parameters are publicly available as a *Kepler* legacy sample.

Key words: asteroseismology – techniques: photometric – stars: variable: general

1 INTRODUCTION

Kepler has revolutionized the field of asteroseismology for solar-like oscillations (Gilliland et al. 2010; Chaplin et al. 2010). It has yielded the detection of gravity-mode period spacings in a red giant (Beck et al. 2011; Mosser et al. 2014), enabling probes of interior rotation of red giants (Beck et al. 2012; Mosser et al. 2012b) and distinguishing between hydrogen- and helium-burning cores (Bedding et al. 2011; Mosser et al. 2012a). It has also permitted the determination of ages and fundamental parameters of main-sequence stars as cool as the Sun and hotter (Silva Aguirre et al. 2013), including planet-hosting stars (Huber et al. 2013; Silva Aguirre et al. 2015a; Van Eylen et al. 2018), revealing the most ancient known planetary system, dating back to the earliest stages of the galaxy (Campante et al. 2015).

★ E-mail: benjamin.pope@nyu.edu

A major outcome of the *Kepler* asteroseismology programme is a legacy sample of extremely well characterized stars that can serve as benchmarks for future work (Lund et al. 2016; Silva Aguirre et al. 2016). Asteroseismological studies with *Kepler* complement other probes of stellar physics well: for example, the APOKASC sample of 1916 spectroscopically- and asteroseismically-characterized red giant stars (Pinsonneault et al. 2014). For this APOKASC sample, Hawkins et al. (2016c) have been able to extract precise elemental abundances by fitting spectroscopic data with $\log g$ and $T_{\rm eff}$ fixed to asteroseismically-determined values. It is necessary to calibrate such a study against benchmark stars with very precisely-determined parameters, which in practice requires nearby bright stars that are amenable to very high signal-to-noise spectroscopy plus asteroseismology (Creevey et al. 2013), parallaxes (Hawkins et al. 2016a), and/or interferometry (Casagrande et al. 2014; Creevey et al. 2015). This is especially important in the context of the *Gaia* mission (Gaia Collaboration et al. 2016), which has recently put out its second data release of 1,692,919,135 sources, including 1,331,909,727 with parallaxes (Gaia Collaboration et al. 2018). These data will form the basis of many large surveys and it is vital that they are calibrated correctly. To this end, 34 FGK stars including both giants and dwarfs have been chosen as *Gaia*-ESO benchmark stars for which metallicities (Jofré et al. 2014), effective temperatures and asteroseismic surface gravities (Heiter et al. 2015), and relative abundances of α and iron-peak elements (Jofré et al. 2015) have been determined. This includes only four main sequence stars much cooler than the Sun, due to the paucity of such stars with asteroseismology. This has been accompanied by the release of high resolution spectra (Blanco-Cuaresma et al. 2014) and formed the basis of extensions to lower metallicities (Hawkins et al. 2016b), stellar twin studies (Jofré 2016) and comparisons of stellar abundance determination pipelines (Jofré et al. 2017). Furthermore, by combining asteroseismology with optical interferometry, it has been possible to determine fundamental parameters of main-sequence and giant stars with unprecedented precision (Huber et al. 2012; White et al. 2013, 2015).

Brighter *Kepler* stars are therefore ideal benchmark targets, since photometry can be most easily complemented by *Gaia* parallaxes, interferometric diameters, and high resolution spectroscopy. Unfortunately, the *Kepler* field was deliberately placed to minimize overall the number of extremely bright stars on the detectors, so that only a dozen stars brighter than 6th magnitude landed on silicon (Koch et al. 2010). This was because stars brighter than $Kp \sim 11$ saturate the CCD detectors, with their flux distributed along a bleed column and rendering those pixels otherwise unusable. Furthermore, due to the limited availablility of bandwidth to download data from the spacecraft, only $\sim 5.7\%$ of pixels on the *Kepler* detectors are actually downloaded in any one Quarter (Jenkins et al. 2010). The result of these two target selection constraints is that photometry was obtained for most of the mission for only 35 stars brighter than $Kp < 7$ in the *Kepler* field, while 17 targets in this range were observed for less than half the mission and 29 targets brighter than this threshold were entirely ignored. The availability of *Kepler* data remains significantly incomplete down to fainter magnitudes, and in this work we consider $Kp = 9$ to be an arbitrary cutoff for bright stars of interest. In the *K2* mission (Howell et al. 2014), very saturated stars have been observed with 'halo photometry' using unsaturated pixels in a specially-determined region around bright stars, including the Pleiades (White et al. 2017), Aldebaran (Farr et al. 2018), and ρ Leonis (Aerts et al. 2018b). Unfortunately, in the legacy *Kepler* sample, photometry of such saturated stars was rarely attempted.

Kolodziejczak & Caldwell (2011) noted a way to obtain photometry of every target on-silicon in *Kepler* using a data channel normally used for calibration, even if active pixels were not allocated and downloaded. *Kepler* employs an inter-line transfer CCD as its detector, which successively shuffles each row of pixels down to the edges of the chip to be read out. Because the *Kepler* camera lacks a shutter, the detector is exposed to light during the readout process, with the result that fluxes in each pixel are contaminated by light collected from stars in the same column. This is a particularly serious issue for faint stars in the same detector column as brighter stars, and it is important to calibrate this at each readout stage. Six rows of blank 'masked' pixels were allocated in each column to measure the smear bias; furthermore, six 'virtual' rows were recorded at the end of the readout, with the result that twelve rows of pixels sample the smear bias in each column. Kolodziejczak & Caldwell (2011) realized that these encode the light curves of bright targets in a 1D projection of the star field. The masked and virtual smear registers each receive $\sim 1/1034$ of the incident flux in each column. If this is dominated by the light from a single star, the flux combining both smear registers is equivalent to that of a star ~ 6.8 times fainter.

In Pope et al. (2016), we demonstrated a method for extracting precise light curves of bright stars in *Kepler* and *K2* from these collateral data, and presented light curves of a small number of variable stars as examples to illustrate this method. In this paper we present smear light curves of all unobserved or significantly under-observed stars brighter than $Kp = 9$ in the *Kepler* field. This sample mostly consists of red giants and hot stars, containing only one G dwarf. We find no transiting planets, but detect one new eclipsing binary, and measure solar-like oscillations in 34 red giants. We do not model main sequence stars in great detail, but provide some discussion and initial classification of interesting variability. For the oscillating red giants that constitute the bulk of the sample, we determine the asteroseismic parameters $\nu_{\rm max}$ and $\Delta\nu$, and therefore stellar masses and $\log g$ measurements. We have also obtained high-resolution optical spectroscopy of 63 stars, predominantly giants, with the Tillinghast Reflector Échelle Spectrograph (TRES). For the 34 stars with both spectroscopy and asteroseismic parameters we derive fundamental stellar parameters and elemental abundances. These asteroseismic constraints can be compared to those from *Gaia*, offering the opportunity both to test asteroseismic scaling relations and combine both datasets to refine the benchmark star properties further.

We have made all new data products and software discussed in this paper publicly available, and encourage interested readers to use these in their own research.

2 METHOD

We have obtained smear light curves for our sample of red giant stars with the `keplersmear` pipeline as described in Section 2.2, performed asteroseismology on all of these to extract $\nu_{\rm max}$ and therefore $\log g$ as described in Section 2.3, and combined these with TRES spectra to obtain chemical abundances as described in Section 2.4.

2.1 Sample

We selected as our sample all stars on-silicon in *Kepler* with $Kp < 9$ that were targeted for fewer than an arbitrary 8 quarters, the majority of which were previously entirely missing. Sixteen stars were to some extent observed conventionally: HD 174020 was targeted in LC for Q2, 6, 10, and 14; HD 175841 for Q11-12, 14-16, with SC for Q3; HD 176582 for Q12-13; HD 178090 for Q1, 3, and 10; HD 180682 for Q0, 3, and 7; HD 181069 for Q1, 10, 13, 14, and 17; HD 181878 for Q14-17; HD 182694 for Q2; HD 183124 for even quarters; HD 185351 for Q1-3 and with SC for Q16; HD 186155 for only Q1; HD 187217 for Q14-17; HD 188252 for only Q13; HD 189013 with SC for Q3 as a γ Dor; V380 Cyg for Q11 and with SC for Q7, 9, 10, 12-17; and V819 Cyg for Q14, 16 and 17. A number of these lay at the edge of a detector, with the result that in some cadences the centroid of the star did not lie on the chip; light curves from these targets were found to be of extremely low quality and all of these stars were discarded. After applying these criteria we obtained a list of 102 targets, which are listed in Table 1 with their *Kepler* magnitude Kp together with their spectral type from SIMBAD, *Gaia* DR2 apparent G magnitudes and $Bp - Rp$ colours, *Gaia* DR2 calibrated distances from Bailer-Jones et al. (2018), variability classification and availability of TRES spectroscopy. The *Kepler* spacecraft rotates between quarters, so that it cycles through four orientation 'seasons' each rotated from the last by 90°. Some stars did not land on silicon for all seasons: we have only one season of HD 179394; two for HD 187277, HD 226754, V554 Lyr, and BD+47 2891; and three for BD+43 3064. The addition of our sample to the conventionally-observed stars makes the *Kepler* survey magnitude-complete down to $Kp = 9$ for all stars on-silicon.

Figure 1 shows these stars on a colour-magnitude diagram using *Gaia* $Bp - Rp$ and absolute G magnitudes and *Gaia* DR2 calibrated distances (Bailer-Jones et al. 2018), overlaid on the *Kepler* sample from the Bedell `gaia-kepler.fun` crossmatch. The smear targets in this diagram appear to have not merely higher apparent brightnesses than the general *Kepler* population, but also higher intrinsic luminosities. While this could simply arise from being selected for their apparent brightness, it is worth considering whether this is because of a bias in their parallax measurements. While *Gaia* parallaxes for very bright stars can be subject to systematic error, we have compared these to those found by *Hipparcos* (van Leeuwen 2007), and found close agreement for the brightest stars, with a scatter that increases with magnitude. We therefore suggest that parallax bias is not the reason for the smear sample sitting above the remainder of the *Kepler* sample.

We identify the evolutionary state of stars in the main sequence versus evolved stars first from the *Gaia* colour-magnitude diagram in Figure 1. Taking a cutoff in *Gaia* $Bp - Rp > 1$, we identify 66 of these stars as evolved systems, and the remaining 36 lie apparently on the main sequence.

The coolest main sequence star, BD+43 3068, is a G0 dwarf with a G magnitude of 8.3 and a distance of 53.8 ± 0.1 pc, and it is therefore surprising that it was not included in the nominal *Kepler* survey as a solar analogue. It is possible that it was previously misidentified as a giant. Regrettably, it is only possible to reconstruct a light curve with the 30 minute long cadence and therefore it is not possible to do asteroseismology on this bright, nearby solar-like star. Its light curve shows neither rotational modulation (as determined by its featureless autocorrelation) nor evidence for transits.

Considering stars lying close to the main sequence, from the *Kepler* power spectrum we identify solar-like oscillations in HD 182354 and HD 176209 at frequencies consistent with them being subgiants or contaminated with flux from red giants.

2.2 Photometry

In preparing light curves of the *Kepler* smear stars, we have followed the methods described in Pope et al. (2016), with some improvements. We selected our input RA and Dec values from the *Kepler* Input Catalog (KIC) (Brown et al. 2011), and queried MAST to find the corresponding mean pixel position for a given *Kepler* quarter. We then measured the centroid of smear columns in the vicinity, and used these values to do raw aperture photometry. We found that the cosine-bell aperture used for raw photometry in Pope et al. (2016) can in some light curves introduce position-dependent systematics and jumps. We instead in this work have applied a super-Gaussian aperture, $A \propto \exp \dfrac{-(x - x_0)}{w}^4$, where x_0 is the centroid and w a width in pixels. The very flat top of this function helps avoid significant variation with position, while still smoothly rolling off at the edges to avoid discontinuous artefacts. This is calculated on a grid of $10\times$ subsampled points in pixel space so that the sharply varying edge changes column weights smoothly as a function of centroid. We have then extracted photometry using apertures with a range of widths $w \in \{1.5, 2, 3, 4, 5\}$ pixels.

From this raw photometry a background light curve was subtracted, which corrects for time-varying global systematics. Whereas in Pope et al. (2016) we subtracted a background estimate chosen manually, for this larger set of light curves, we have now chosen the lowest 25% of pixels by median flux as being unlikely to be contaminated by stars, and taken our background level to be the median of this at each time sample. To denoise this, we fit a Gaussian Process with a 30-day timescale squared exponential kernel using GEORGE (Ambikasaran et al. 2015), and our final background light curve is taken to be the posterior mean of this GP.

The dominant source of residual systematic errors in nominal *Kepler* time series is a common-mode variation primarily due to thermal changes on board the spacecraft, an issue which is traditionally dealt with by identifying and fitting a linear combination of systematic modes (Twicken et al. 2010; Stumpe et al. 2012; Smith et al. 2012; Petigura & Marcy 2012). We have adopted the same approach here, using the *Kepler* Pre-search Data Conditioning (PDC) Cotrending Basis Vectors (CBVs) available from MAST, finding least-squares fits of either the first 4 or 8 CBVs to each light curve. This can subtract astrophysical signals on long timescales, such that we use and recommend 4 CBV light curves for stars with variability on timescales longer than ~ 5 days, or indeed raw uncorrected lightcurves for stars variable at high amplitude on $\sim$ quarter timescales, but otherwise we recommend the 8 CBV light curves. There is some room for improvement here by simultaneously modelling astrophysical and instrumental variations, but this is beyond the scope of this paper. In the following, we will use the light curves with the lowest 6.5 hr Combined Differential Photometric Precision (CDPP) (Christiansen et al. 2012) out of all apertures, as calculated with the K2SC implementation (Aigrain et al. 2016). This is not necessarily the optimal choice for all red giants, especially those with oscillations on a 6.5 h timescale, but is a reasonable proxy nevertheless for white noise and leads to satisfactory results upon visual inspection of the present sample.

Because the smear data are collected along an entire CCD column, there is the risk of contamination from other bright stars. This is especially true in doing asteroseismology of red giants, where the low-amplitude stochastically-excited oscillations can be washed out in a power spectrum by the coherent high amplitude variations of a classical pulsator, even if the background star is much fainter. We can assess the importance of this contamination by considering the differences between odd and even quarters: because the *Kepler* spacecraft rotates 90° between successive quarters, any contaminant will lie in the same column as a smear target only every second quarter, falling in the other quarters in the same row but not necessarily

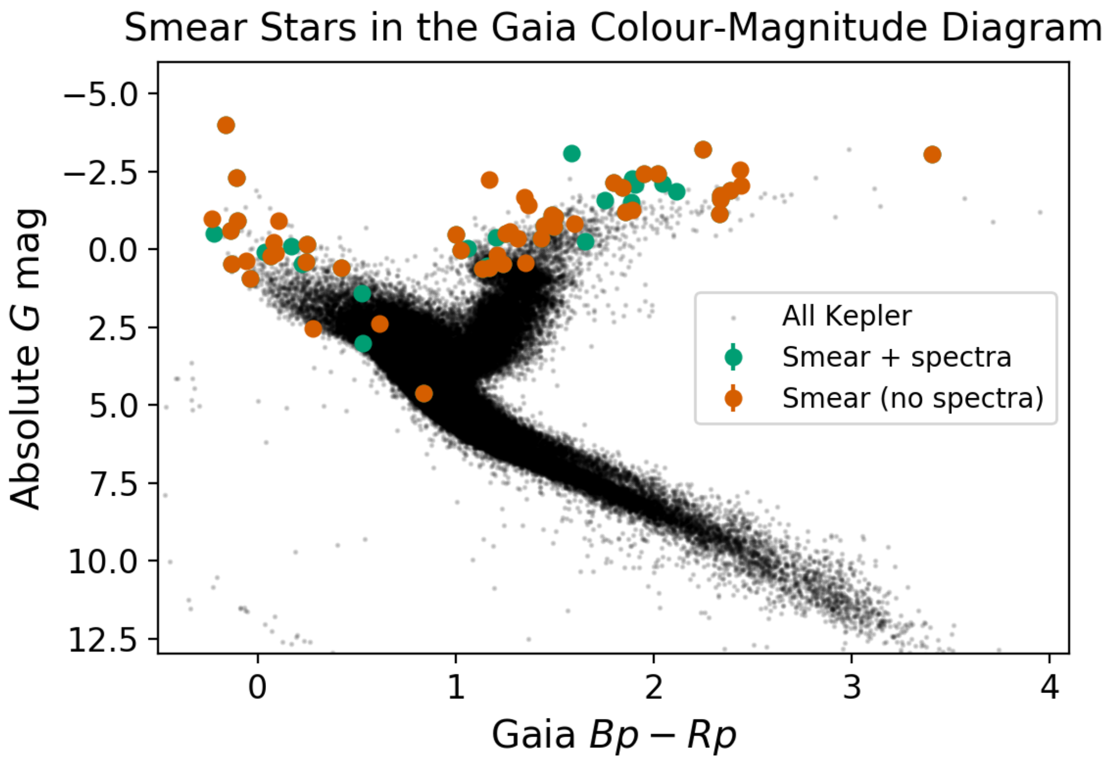

Figure 1. *Gaia* colour-magnitude diagram of the Smear Campaign stars (orange and teal) overlaid on the sample of *Kepler* stars with *Gaia* parallax SNR > 25 (black), using the Bedell `gaia-kepler.fun` crossmatch and *Gaia* DR2 calibrated distances from Bailer-Jones et al. (2018). The smear sample includes giants and hot main-sequence stars. Those giants for which TRES spectroscopy have been obtained are highlighted in teal. An interactive version of this diagram is available as supplementary material from the journal or at `benjaminpope.github.io/data/cmd_smear.html`.

the same column. We have therefore generated Lomb-Scargle periodograms (Lomb 1976; Scargle 1982) of each light curve, clipped for outliers, and considering only odd and even quarters, and both visually inspected these for significant differences. In the great majority of cases they closely resemble one another, indicating that contamination is at worst a minor effect. In order to better quantify this, we compute the inner product of normalized periodograms of the odd and even quarters each smoothed with a 3-element Gaussian kernel. If this overlap integral is 1, then the power spectra are identical; substantial departures from unity may be caused by real nonstationary or long-period stellar variation, noise, or gain or contamination differences between the seasons. We find that the distribution of overlaps is strongly peaked around ~ 0.91, with a tail of 22 stars showing overlap < 0.9. We investigate these further, finding that in not all of these cases is there an obvious problem, for example the classical pulsator HD 175841 in which amplitudes of several pulsations have changed but the overall distribution seems very similar, in which we conclude that the variation is probably astrophysical or an artefact of our data processing.

In the case of HD 181878, a red giant, there is clear and significant contamination from an M giant, as is seen in Figure 2. Likewise HD 183383 shows two different stars, depending on the quarter: some parts are likely from an ellipsoidal variable with a period of 6.46 days, other parts are from an RR Lyrae pulsator. Between seasons, there is an extra hump of power near the red giant oscillations in HD 175740; extra low frequency power in HD 180658; one coherent peak in HD 182694; high frequency contamination in HD 181597 possibly from an EB; and a very significant difference in amplitude between seasons for BD +39 3882. In other cases visual inspection does not show severe contamination, but in all cases we recommend that users of these light curves carefully check for differences between odd and even quarters.

2.3 Asteroseismology

Among the 66 red giants identified in this sample, for 32 the timescale of their variability is of the same order as a *Kepler* quarter and they are thus badly affected by systematics and systematics correction. In Table 1 we have noted these as ‘long-period variables’ (LPVs), without specifically meaning these are LPVs by a particular astrophysical definition, and they are discussed further in Section 3.1.3. For the 34 giants for which there is high-SNR shorter-timescale variability, we have attempted to extract the asteroseismic parameters $\nu_{\rm max}$ and $\langle\Delta\nu\rangle$ (Kjeldsen & Bedding 1995; Chaplin & Miglio 2013). These constrain fundamental stellar parameters through the approximate scaling relations:

$$\nu_{\rm max} \propto \frac{g}{g_\odot} \cdot \left(\frac{T_{\rm eff}}{T_{\rm eff\odot}}\right)^{\frac{1}{2}} \tag{1}$$

and

$$\langle\Delta\nu\rangle \propto \sqrt{\langle\rho\rangle} = \sqrt{MR^{-3}} \tag{2}$$

We have followed the method of Davies & Miglio (2016), obtaining a Lomb-Scargle periodogram of the smoothed time series according to the method of García et al. (2011). The poste-

Table 1. The full set of underobserved and unobserved stars for which new light curves have been produced in this smear catalogue. Calibrated *Gaia* distances are from Bailer-Jones et al. (2018). Some objects, such as HD 185351, were observed in long cadence in some quarters and short cadence in others, and this is noted accordingly. The eclipsing binary V2083 Cyg was detected by *Gaia*, but a parallax could not be obtained in DR2, possibly due to binary motion. Variability classes are determined by inspection, having their usual abbreviations. EV denotes an ellipsoidal variable, and RM rotational modulation, though these two can appear similar. α^2 CVn variables are chemically-peculiar stars with rotational spot modulation, and are noted separately from RM without chemical peculiarity. γ Dor/δ Sct denotes a γ Dor/δ Sct hybrid, not uncertainty. H+S denotes a 'hump and spike' star. Question marks indicate uncertainty, and dashes – that no significant variability is observed.

Object	KIC	Spectral Type (SIMBAD)	Kp (mag)	G (mag)	$Bp - Rp$ (mag)	*Gaia* Distance (pc)	TRES	Variability Class
14 Cyg	7292420	B9III	5.490	4.882	1.091	$41.2^{+0.1}_{-0.1}$	–	H+S
BD+36 3564	1575741	K5	8.128	4.923	0.529	$50.6^{+0.4}_{-0.4}$	–	RG
BD+39 3577	4989821	G5	8.131	5.152	1.171	$81.5^{+0.6}_{-0.6}$	–	RG
BD+39 3882	4850372	F5	8.259	5.279	0.107	$172.6^{+3.3}_{-3.2}$	–	?
BD+42 3150	7091342	K0	8.350	5.370	-0.055	$194.3^{+7.0}_{-6.6}$	–	?
BD+42 3367	7447756	M0	7.271	5.410	-0.106	$347.3^{+13.0}_{-12.1}$	–	LPV
BD+42 3393	6870455	K5	7.664	5.313	2.047	$306.4^{+10.3}_{-9.6}$	–	LPV
BD+43 3064	8075287	K5	8.284	5.598	1.061	$133.1^{+0.7}_{-0.7}$	–	RG
BD+43 3068	8006792	G0	8.308	5.632	-0.062	$1044.7^{+116.6}_{-95.6}$	–	–
BD+43 3171	7810954	M0	8.373	5.176	2.250	$475.2^{+35.1}_{-30.7}$	–	LPV
BD+43 3213	7747499	K5	8.311	5.881	0.246	$125.2^{+6.2}_{-5.7}$	–	LPV
BD+47 2825	10337574	K0	8.251	5.864	-0.276	$1000.6^{+82.6}_{-71.1}$	–	EB
BD+47 2891	10347606	K0	8.680	5.985	1.283	$135.8^{+0.3}_{-0.3}$	–	RG
BD+48 2904	11085556	K0	8.487	6.055	1.645	$263.5^{+3.9}_{-3.8}$	–	RG
BD+48 2955	10988024	K2	7.961	6.091	1.584	$683.8^{+12.4}_{-11.9}$	–	RG
HD 174020	7800227	K5	6.753	5.919	1.905	$397.8^{+6.8}_{-6.6}$	–	RG
HD 174177	9630812	A2IV	6.575	5.228	2.725	$288.9^{+13.1}_{-12.0}$	–	?
HD 174676	7420037		7.481	6.144	1.448	$238.9^{+1.5}_{-1.4}$	–	LPV
HD 174829	7339102	K0	6.967	6.264	1.237	$144.2^{+0.6}_{-0.6}$	–	RG
HD 175132	6020867	B9IIIpSi	6.362	6.258	1.168	$499.2^{+7.2}_{-7.0}$	–	α^2 CVn
HD 175466	7340766	K2	6.165	6.160	-0.217	$345.1^{+5.6}_{-5.4}$	–	LPV
HD 175740	6265087	G8III	5.212	6.291	1.253	$228.9^{+1.7}_{-1.7}$	–	RG
HD 175841	4989900	A2	6.885	6.242	-0.063	$333.3^{+5.9}_{-5.7}$	–	γ Dor/δ Sct
HD 175884	6584587	K0	6.210	6.243	-0.160	$1114.0^{+70.9}_{-63.0}$	–	RG
HD 176209	9327530	A0	7.437	6.208	-0.041	$571.1^{+18.2}_{-17.2}$	–	?
HD 176582	4136285	B5V	6.510	6.345	1.273	$243.2^{+1.8}_{-1.8}$	–	α^2 CVn
HD 176626	7943968	A2V	6.933	6.395	1.176	$160.7^{+0.8}_{-0.8}$	–	RM
HD 176894	6267965	F0	7.700	6.171	2.031	$409.4^{+3.8}_{-3.7}$	–	γ Dor
HD 177697	4994443	K5	7.300	6.248	1.892	$317.7^{+2.7}_{-2.7}$	–	RG
HD 177781	2970780	G5	7.744	6.383	-0.232	$298.6^{+3.9}_{-3.8}$	–	γ Dor/δ Sct
HD 178090	6675338	K5	6.758	6.483	0.119	$223.9^{+1.7}_{-1.6}$	–	LPV
HD 178797	10064283	K0	7.312	6.532	1.486	$295.8^{+2.5}_{-2.5}$	–	RG
HD 178910	11288450	K2	7.864	6.587	1.003	$259.5^{+1.8}_{-1.8}$	–	RG
HD 179394	7105221	B8	7.575	6.600	1.754	$433.1^{+4.2}_{-4.1}$	–	–
HD 179395	6593264	B9	7.168	6.658	-0.003	$139.6^{+1.1}_{-1.1}$	–	α^2 CVn
HD 179396	3838362	K2	8.001	6.549	1.892	$583.0^{+8.5}_{-8.3}$	–	RG
HD 179959	10265370	K0	6.280	6.696	1.798	$585.0^{+9.1}_{-8.9}$	–	RG
HD 180312	4551179	K0II	7.970	6.797	0.172	$241.0^{+2.1}_{-2.1}$	–	RG
HD 180475	11656042	K2	7.664	6.813	0.351	–	–	RG
HD 180658	6195870	K0	7.932	6.840	0.225	$188.8^{+6.4}_{-6.0}$	–	RG
HD 180682	5177450	K0	6.617	6.530	2.116	$476.9^{+5.9}_{-5.8}$	–	LPV
HD 181022	3946721	K5	6.496	6.841	0.035	$224.8^{+1.8}_{-1.7}$	–	LPV
HD 181069	4049174	K1III	6.279	6.852	0.059	$217.8^{+3.4}_{-3.3}$	–	RG
HD 181097	4149233	K0	7.920	6.855	0.421	$180.0^{+1.0}_{-1.0}$	–	RG
HD 181328	12456737	M1	7.182	6.862	0.252	$254.5^{+4.1}_{-4.0}$	–	LPV
HD 181521	5180075	A0	6.939	6.928	1.391	$355.0^{+3.5}_{-3.4}$	–	γ Dor/δ Sct
HD 181596	11910615	K5III	7.050	5.403	3.406	$494.7^{+34.9}_{-30.6}$	–	RG
HD 181597	11555267	K1III	6.040	6.863	1.841	$591.1^{+8.1}_{-7.8}$	–	RG
HD 181681	5092997	K4III	6.864	7.070	0.067	$233.9^{+1.7}_{-1.7}$	–	RG
HD 181778	7816792	K0	7.545	7.034	-0.221	$321.5^{+3.7}_{-3.6}$	–	RG
HD 181878	4830109	G5	6.698	6.614	2.334	$353.9^{+3.3}_{-3.3}$	–	RG
HD 181880	3337423	K	7.982	6.719	2.337	$492.9^{+5.5}_{-5.4}$	–	RG

Table 1 – *continued* The full set of underobserved and unobserved stars for which new light curves have been produced in this smear catalogue. Calibrated *Gaia* distances are from Bailer-Jones et al. (2018).

Object	KIC	Spectral Type (SIMBAD)	Kp (mag)	G (mag)	$Bp - Rp$ (mag)	*Gaia* Distance (pc)	TRES	Variability Class
HD 182354	2156801	K0	6.320	7.143	-0.055	$226.5^{+2.4}_{-2.3}$	–	RG
HD 182531	11188366	K5	7.955	7.145	-0.037	$175.5^{+2.6}_{-2.5}$	–	RG
HD 182692	10728753	K0	7.310	6.992	2.020	$762.0^{+15.8}_{-15.2}$	–	RG
HD 182694	7680115	G7IIIa	5.722	6.764	2.338	$472.0^{+5.4}_{-5.3}$	–	RG
HD 182737	1572070	A0	7.820	7.247	1.227	$226.6^{+1.3}_{-1.3}$	–	RM
HD 183124	8752618	G8II	6.441	7.249	1.478	$406.1^{+4.8}_{-4.7}$	–	RG
HD 183203	12208512	K5	6.928	7.189	-0.135	$361.2^{+6.4}_{-6.1}$	–	LPV
HD 183362	2715115	B3Ve	6.394	7.324	1.345	$629.9^{+11.4}_{-11.0}$	–	γ Dor, H+S
HD 183383	6777469	B9	7.640	6.784	2.443	$587.8^{+13.1}_{-12.6}$	–	?
HD 184147	9651435	B9IV	7.251	7.365	0.091	$282.2^{+2.7}_{-2.7}$	–	?
HD 184215	11031549	B8	7.321	7.440	2.434	$993.3^{+26.7}_{-25.4}$	–	SPB
HD 184483	7756961	M5	7.246	6.917	2.388	$581.7^{+9.2}_{-8.9}$	–	LPV
HD 184565	6047321	K0	7.972	7.514	1.315	$374.5^{+3.4}_{-3.4}$	–	LPV
HD 184787	6528001	A0V	6.757	7.475	-0.100	$476.2^{+12.2}_{-11.6}$	–	H+S
HD 184788	6129225	B9	7.249	7.464	0.282	$96.9^{+0.4}_{-0.4}$	–	RM
HD 184875	6954647	A2V	5.403	7.451	-0.185	$1866.1^{+138.1}_{-120.6}$	–	γ Dor
HD 185117	9094435	K5	7.696	7.537	0.081	$357.1^{+5.5}_{-5.3}$	–	LPV
HD 185286	7966681	K5	6.151	7.595	1.489	$546.1^{+8.0}_{-7.8}$	–	RG
HD 185351	8566020	G8.5IIIbFe-0.5	5.034	7.414	1.952	$929.0^{+25.9}_{-24.5}$	–	RG
HD 185397	3455268	A5	6.953	7.472	1.921	$817.7^{+14.8}_{-14.3}$	–	δ Sct
HD 185524	8960196	K2	8.022	7.610	0.530	$82.8^{+0.2}_{-0.2}$	–	LPV
HD 186121	7456762	M3III	5.773	7.546	1.888	$651.0^{+12.0}_{-11.6}$	–	LPV
HD 186155	9163520	F5II-III	5.055	7.701	1.024	$296.2^{+2.6}_{-2.5}$	–	H+S
HD 186255	4937492	A3	6.966	7.758	0.421	$460.3^{+6.7}_{-6.5}$	–	δ Sct
HD 186727	12316020	M0	7.499	7.702	1.652	$391.8^{+6.1}_{-5.9}$	–	LPV
HD 186994	8766240	B0III	7.585	7.848	1.346	$291.3^{+2.4}_{-2.4}$	–	EB
HD 187217	11824273	K0	6.399	7.848	1.434	$434.3^{+6.2}_{-6.0}$	–	RG
HD 187277	6967644	A0	7.579	7.871	1.256	$282.2^{+2.3}_{-2.3}$	–	–
HD 187372	10679281	M1III	5.672	7.859	1.502	$599.3^{+9.2}_{-8.9}$	–	LPV
HD 188252	10683303	B2III	6.007	7.899	1.549	$589.4^{+11.6}_{-11.1}$	–	SPB
HD 188537	9110718	K0	7.382	7.834	1.162	$290.5^{+2.4}_{-2.4}$	–	RG
HD 188629	8710324	K5	7.743	7.943	1.024	$380.9^{+4.3}_{-4.2}$	–	LPV
HD 188875	5041881	K2	6.164	7.940	1.498	$541.2^{+10.1}_{-9.7}$	–	RG
HD 189013	10096499	A2	6.922	7.970	1.244	$321.2^{+2.7}_{-2.6}$	–	γ Dor
HD 189178	5219588	B5V	5.552	7.953	1.368	$753.4^{+15.9}_{-15.2}$	–	SPB, H+S
HD 189636A	10298067		8.025	8.118	1.211	$384.7^{+6.0}_{-5.8}$	–	?
HD 189636B	10298061		8.107	8.061	1.207	$327.0^{+3.0}_{-2.9}$	–	?
HD 189684	9305008	A5III	5.982	8.024	1.316	$376.4^{+4.9}_{-4.7}$	–	EV
HD 189750	8521828	K0	8.052	8.041	1.544	$547.1^{+11.6}_{-11.1}$	–	?
HD 190149	8262528	M0II-III	6.488	8.090	1.134	$311.7^{+2.7}_{-2.7}$	–	LPV
HD 226754	6234579	K2	7.829	8.092	-0.129	$335.7^{+4.6}_{-4.5}$	–	RG
V2079 Cyg	8818020	B8V	7.174	8.236	1.329	$485.8^{+7.3}_{-7.1}$	–	α^2 CVn
V2083 Cyg	10342012	A3	6.902	8.159	0.616	$143.3^{+0.7}_{-0.7}$	–	EB
V380 Cyg	5385723	B1.1III+B2.5/3V	5.771	8.203	1.599	$641.0^{+20.3}_{-19.1}$	–	EB
V398 Lyr	4042516	M3	7.024	8.268	0.839	$53.8^{+0.1}_{-0.1}$	–	RG
V543 Lyr	5429169	B3V	6.299	8.139	1.876	$948.8^{+25.8}_{-24.5}$	–	SPB
V546 Lyr	6267345	M3III	7.385	8.315	1.206	$546.0^{+32.5}_{-29.1}$	–	LPV
V547 Lyr	5429948	M4-IIIa	6.199	8.178	1.858	$751.5^{+17.2}_{-16.5}$	–	LPV
V554 Lyr	5001462		8.179	8.439	1.355	$400.9^{+5.4}_{-5.3}$	–	α^2 CVn
V819 Cyg	10618721	B0.5IIIn	6.381	8.625	1.291	$262.8^{+1.7}_{-1.6}$	–	SPB

rior distribution of the asteroseismic parameters is obtained with a Markov Chain Monte Carlo fit to the smoothed periodogram, applying the combined granulation and oscillation model of Kallinger et al. (2014). This consists of two Harvey profiles for the granulation (Harvey 1985), a Gaussian envelope for the stellar oscillations, and a white noise background for instrumental noise. The marginal posterior distribution for the oscillation envelope is well-approximated by a single Gaussian, and we have taken its median and standard deviation to be our estimates for $\nu_{\max}$ and its uncertainty.

To estimate $\Delta\nu$, we have divided the power spectrum through by the granulation and noise models to obtain a signal-to-noise spectrum, and fit a sum of Lorentzians separated by mean large ($\Delta\nu$) and small ($\delta\nu$) separations to the part of this spectrum in the vicinity of $\nu_{\max}$. In practice, for this dataset, $\delta\nu$ is not constrained, but

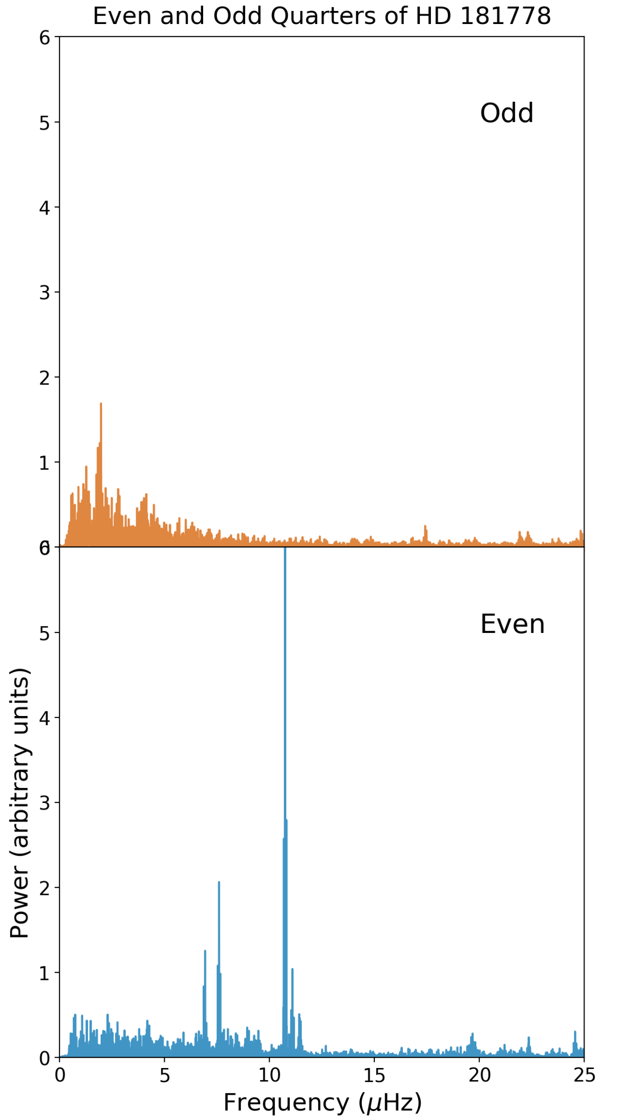

Figure 2. Power spectra of odd and even quarters of HD 181778. It is clear from inspection that while odd quarters have the power spectrum expected of a giant star, even quarters have very high amplitude coherent oscillations typical of an M giant.

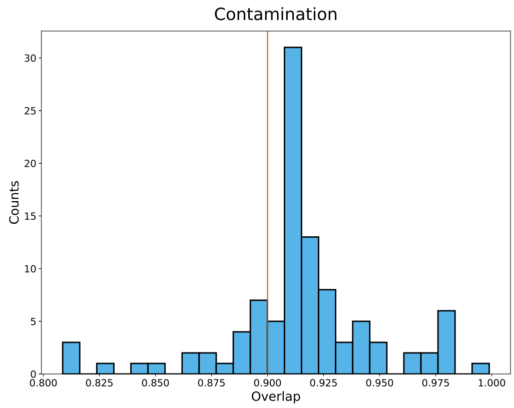

Figure 3. Histogram over overlap integrals of smoothed periodograms of odd and even quarters for each star in the sample. The peak at ~ 0.91 contains normal stars with limited contamination; we investigate the 22 stars with overlaps below 0.9 for which there is a significant risk of contamination.

mean $\langle \Delta\nu \rangle$ is typically well-constrained and its posterior marginal distribution is well-represented by a single Gaussian as with $\nu_{\rm max}$.

We obtain good estimates of these asteroseismic parameters for 34 targets, presented in Table 2. In the remainder of cases, as noted above, we find that the very-low-frequency ($\lesssim 2\mu$Hz) oscillations are affected by filter artefacts from detrending, and we are not able to obtain good estimates for these stars.

Once $\nu_{\rm max}$ has been estimated, we have used Equation 1, the asteroseismic scaling relation for $\nu_{\rm max}$ (Brown et al. 1991; Kjeldsen & Bedding 1995), to estimate $\log g$ in order to inform extraction of chemical abundances from spectra. Using the initial spectroscopic estimate of $T_{\rm eff}$, which is not significantly informed by $\nu_{\rm max}$, uncertainties in $\nu_{\rm max}$ are propagated with Monte Carlo sampling.

For eight stars, we have found that the asteroseismic fit is unsatisfactory: for BD+39 388 we cannot detect the expected oscillations; for BD+43 3064 there are significant peaks but these are not consistent with the pattern expected from a red giant; for HD 179959 and HD 187217 we suspect contamination with the oscillations of a second giant, which is hard to remove from smear light curves; while for HD 188629, HD 188639 and HD 188875 we can extract a $\nu_{\rm max}$ but not a robust $\Delta\nu$. One star in our sample, HD 185351, has a mode envelope that is not well fit by our model. The smear light curve for this star has already been published by Hjørringgaard et al. (2017), who showed with detailed asteroseismic modelling that it had a zero-age main sequence mass of $\sim 1.60 M_\odot$ (a so-called 'retired A star') and used it to calibrate the convective overshoot parameter for low-luminosity red giants. The global asteroseismic modelling presented here should therefore be considered to be superseded by the more detailed model of Hjørringgaard et al. (2017).

2.4 Spectroscopy

We have obtained high-resolution spectroscopy with TRES for 63 stars, mainly giants, in order to constrain stellar parameters and elemental abundances. Operating with spectral resolving power $R = 44000$, we have obtained spectra with signal-to-noise ratios (SNRs) of tens to hundreds per resolution element. Although this resolution and SNR are sufficient for an exploratory study, for more detailed analysis it will be desirable to use APOGEE or similar instruments to obtain greater spectral coverage. From this observing run we have 34 unique targets with seismic $\log g$ and spectra, one more star than the *Gaia*-ESO benchmark set and a significant addition to the ensemble of bright red giants with asteroseismic parameter determinations. Due to observing constraints, we were unable to obtain spectra for BD+42 3150, BD+48 2904, HD 176209, HD 182354, HD 189636AB, or HD 189750.

To derive stellar parameters from our TRES spectra, we initially ran the Stellar Parameter Classification (SPC: Buchhave et al. 2012) code to determine $T_{\rm eff}$ and $\log g$, using the SPC $T_{\rm eff}$ to inform the asteroseismic estimation of $\log g$ from $\nu_{\rm max}$. For deriving abundances, $T_{\rm eff}$ is fixed from the results of an initial SPC fit, while $\log g$ is fixed to the seismic values. The other stellar atmospheric parameters including the microturbulent velocity ($v_{\rm mic}$), and broadening (convolution by $V_{\rm mac}$, $v_{\sin i}$ and the instrumental line profile) as well as [Fe/H] and chemical abundances for 20 chemical species are derived using the Brussels Automatic Code for Characterizing High accUracy Spectra (BACCHUS: Masseron et al. 2016), and

Table 2. Bulk asteroseismic parameters $\Delta\nu$, ν_{max}, and ϵ for the red giant sample as discussed in Section 2.3.

Object	$\Delta\nu$ (μHz)	ν_{max} (μHz)	ϵ
BD+36 3564	0.95 ± 0.03	5.08 ± 0.10	0.83 ± 0.20
BD+39 3577	1.68 ± 0.01	13.27 ± 0.32	0.74 ± 0.06
BD+42 3150	4.22 ± 0.03	38.32 ± 0.96	0.70 ± 0.07
BD+43 3171	0.42 ± 0.05	1.98 ± 0.05	0.80 ± 0.17
BD+43 3213	0.49 ± 0.01	2.56 ± 0.06	1.01 ± 0.07
BD+48 2904	2.85 ± 0.01	23.13 ± 0.72	0.86 ± 0.08
BD+48 2955	0.90 ± 0.01	5.44 ± 0.08	0.81 ± 0.05
HD 174020	0.56 ± 0.02	2.48 ± 0.10	0.89 ± 0.08
HD 174829	1.28 ± 0.01	7.95 ± 0.16	0.78 ± 0.06
HD 175740	5.93 ± 0.01	64.33 ± 0.78	1.00 ± 0.02
HD 175884	1.12 ± 0.01	7.07 ± 0.11	0.96 ± 0.08
HD 176209	4.22 ± 0.08	36.08 ± 0.77	0.87 ± 0.06
HD 178797	1.03 ± 0.02	6.34 ± 0.09	0.74 ± 0.29
HD 178910	3.64 ± 0.02	32.06 ± 0.31	0.83 ± 0.05
HD 179396	3.76 ± 0.02	31.02 ± 0.44	0.92 ± 0.03
HD 180312	4.17 ± 0.02	33.84 ± 0.28	0.96 ± 0.04
HD 180475	0.82 ± 0.00	4.34 ± 0.10	0.68 ± 0.03
HD 180658	4.00 ± 0.02	33.76 ± 0.50	0.90 ± 0.05
HD 180682	0.77 ± 0.05	3.68 ± 0.08	1.07 ± 0.15
HD 181022	0.38 ± 0.01	1.58 ± 0.03	0.70 ± 0.10
HD 181069	4.43 ± 0.01	41.46 ± 0.32	0.90 ± 0.02
HD 181097	1.61 ± 0.02	11.16 ± 0.14	0.72 ± 0.36
HD 181597	3.11 ± 0.01	25.84 ± 0.25	0.97 ± 0.02
HD 181778	2.56 ± 0.02	22.86 ± 0.29	0.72 ± 0.06
HD 181880	1.04 ± 0.01	6.54 ± 0.10	0.76 ± 0.05
HD 182354	2.66 ± 0.01	24.73 ± 0.37	0.74 ± 0.04
HD 182531	1.03 ± 0.00	6.47 ± 0.09	0.86 ± 0.03
HD 182692	4.66 ± 0.01	44.38 ± 0.47	0.87 ± 0.02
HD 182694	5.71 ± 0.01	69.78 ± 1.02	0.94 ± 0.25
HD 183124	4.39 ± 0.01	39.59 ± 0.29	0.95 ± 0.03
HD 185286	0.72 ± 0.01	4.23 ± 0.10	0.73 ± 0.08
HD 188537	1.55 ± 0.01	13.40 ± 0.34	0.72 ± 0.07
HD 189750	4.16 ± 0.04	36.14 ± 0.58	0.94 ± 0.08
HD 226754	1.19 ± 0.01	7.41 ± 0.19	0.74 ± 0.08

the results from this calculation are displayed in Table 3. BACCHUS uses an interpolation scheme through a grid of MARCS model atmospheres (Gustafsson et al. 2008) in combination with TURBOSPECTRUM (Alvarez & Plez 1998; Plez 2012). For the calculation of synthetic spectra, atomic line information has been taken from the fifth version of the Gaia-ESO linelist (Heiter et al., in preparation). Additionally we used the molecular species for CH (Masseron et al. 2014), CN, NH, OH, MgH C_2 (T. Masseron, private communication). The SiH molecular information is adopted from the Kurucz linelists and the information for TiO, ZrO, FeH, CaH from B. Plez (private communication).

Individual elemental abundances are derived by first fixing the stellar atmospheric parameters to those determined above. Spectra are then synthesized in regions centered around an absorption feature of the element we want to derive. The spectra generated will have different [X/Fe] values. A χ^2 minimization procedure is then done to derive the best fitting abundance for each line. The reported abundances are the median [X/Fe] value of the various line regions for a given element. Abundance uncertainties reported are the standard error in the line-by-line abundance ratios. Where only one line exists for a given element, we conservatively assume the standard error is 0.10 dex. In principle, these uncertainties are underestimated because there they do not include the errors driven by imperfect stellar parameter values and other systematic errors arising, for instance, from incorrect line list data. We do note, however, thus use of asteroseismology really reduces the uncertainties caused by the stellar parameters (see Hawkins et al. 2016c, for a longer discussion on this).

To achieve the most precise abundances we have derived them using both with and without a line-by-line differential approach with respect to Arcturus (α Boötis) using the method described by Jofré et al. (2015) and the Arcturus abundances from (Hawkins et al. 2016c). Choosing this method means we do not derive the abundances for neutron capture elements (e.g. Sr, Y, Zr, Ba, La, Nd, Eu) in a differential way because there are no estimated values for these elements at the appropriate benchmark parameters of Arcturus. For these elements we instead derive the chemical abundances in an aboslute way where the solar abundances of Asplund et al. (2005) are assumed. The uncertainty in the abundances are taken a the line-by-line dispersion or assumed to be 0.10 when just one line is available. No abundances for oxygen could be reliably derived for any of the stars in our spectroscopic sample by either method.

3 RESULTS

3.1 Red Giants

We determined physical properties such as mass, radius, and age for the 33 red giants from their atmospheric and asteroseismic observables (see Table) using the BAyesian STellar Algorithm (BASTA Silva Aguirre et al. 2015b, 2017). BASTA compares the observed properties with predictions from theoretical models of stellar evolution, in this case the recently updated BaSTI (a Bag of Stellar Tracks and Isochrones) stellar models and isochrones library (Hidalgo et al. 2018) with overshooting and no mass-loss.

The spectroscopic properties we fit are the effective temperature $T_{\rm eff}$, the metallicity [Fe/H], and the surface gravities $\log g$ from Table 3. These are accompanied by the global asteroseismic properties $\Delta\nu$ and ν_{max} from Table 2. Theoretical predictions of $\Delta\nu$ and ν_{max} are computed using the asteroseismic scaling relation for any point along an evolutionary track or isochrone. For the solar values, we adopt $\nu_{max,\odot}$ = 3090 μHz, $\Delta\nu_\odot$ = 135.1 μHz (Huber et al. 2011), and $T_{\rm eff,\odot}$ = 5777 K.

The accuracy of the asteroseismic scaling relations across different metallicities, effective temperatures, and evolutionary status is currently an active discussion within the field of asteroseismology (see White et al. 2011; Belkacem et al. 2011; Sharma et al. 2016; Viani et al. 2017). We apply the correction by Serenelli et al. (2017) to the large frequency separation relation in Equation **??** as it has been shown to reproduce the results of a number of classical age determination for the open clusters M67 (Stello et al. 2016) and NGC 6819 (Casagrande et al. 2016).

We compare the solutions found using this set of fitting parameter with those found using only spectroscopic input in Figure 4, and we find that the change in median stellar parameters between the two results is small for all analyzed red giants. However, in the comparison plot it becomes visible how adding the asteroseismic constraints to the fit narrows down the parameter space and thus decrease the derived uncertainties.

3.1.1 Chemical Compositions

The chemical composition for each star was measured in the α (Mg, Ti, Si, Ca), odd-Z (Al, V) and Fe-peak (Fe, Ni) elemental

Table 3. Fundamental stellar parameters for the red giant sample as determined jointly by asteroseismology (asteroseismic log g; Section 2.3) and spectroscopy (RV, $T_{\rm eff}$, log g, [M/H], $V \sin i$, SNR, Mass, and Age; Section 2.4.)

Object	RV (km/s)	$T_{\rm eff}$ (K)	log g	[M/H]	$V \sin i$ (km/s)	SNR	Mass ($M_\odot$)	Age (Gyr)
BD+36 3564	−77.84 ± 0.05	4100 ± 50	1.57 ± 0.01	−0.63 ± 0.08	5.54 ± 0.50	71.8	$0.9^{+0.1}_{-0.1}$	$12.4^{+3.6}_{-3.9}$
BD+39 3577	−14.81 ± 0.07	4737 ± 50	2.02 ± 0.01	−0.41 ± 0.08	4.78 ± 0.50	92.8	$2.4^{+0.2}_{-0.2}$	$0.7^{+0.2}_{-0.2}$
BD+42 3150	−26.52 ± 0.07	4776 ± 50	2.48 ± 0.01	−0.19 ± 0.08	4.22 ± 0.50	90.4	$1.4^{+0.1}_{-0.1}$	$2.9^{+1.3}_{-0.7}$
BD+43 3171	−16.32 ± 0.11	3656 ± 50	1.14 ± 0.01	−1.20 ± 0.08	4.54 ± 0.50	68.9	$0.8^{+0.0}_{-0.0}$	$14.8^{+1.3}_{-2.4}$
BD+43 3213	−14.16 ± 0.16	3901 ± 50	1.26 ± 0.01	−0.16 ± 0.08	6.82 ± 0.50	57.3	$1.6^{+0.1}_{-0.1}$	$2.4^{+0.8}_{-0.6}$
BD+48 2904	5.24 ± 0.03	4484 ± 50	2.25 ± 0.01	−0.30 ± 0.08	4.11 ± 0.50	59.8	$1.3^{+0.1}_{-0.1}$	$4.4^{+1.7}_{-1.2}$
BD+48 2955	1.66 ± 0.04	4143 ± 50	1.60 ± 0.01	−0.60 ± 0.08	5.33 ± 0.50	31.7	$1.6^{+0.1}_{-0.1}$	$1.8^{+0.3}_{-0.3}$
HD 174020	−14.84 ± 0.08	3781 ± 50	1.27 ± 0.02	−1.03 ± 0.08	5.38 ± 0.50	120.1	$0.8^{+0.0}_{-0.0}$	$15.6^{+1.4}_{-2.4}$
HD 174829	10.15 ± 0.03	4381 ± 50	1.78 ± 0.01	−0.48 ± 0.08	4.71 ± 0.50	112.2	$1.3^{+0.1}_{-0.1}$	$3.3^{+0.9}_{-0.6}$
HD 175740	−8.81 ± 0.04	4875 ± 50	2.71 ± 0.01	−0.12 ± 0.08	3.90 ± 0.50	169.3	$1.8^{+0.0}_{-0.0}$	$1.6^{+0.2}_{-0.0}$
HD 175884	−34.39 ± 0.07	4306 ± 50	1.72 ± 0.01	−0.41 ± 0.08	4.91 ± 0.50	144.4	$1.6^{+0.1}_{-0.1}$	$2.0^{+0.5}_{-0.3}$
HD 176209	−12.91 ± 0.93	8097 ± 71	2.57 ± 0.01	−0.08 ± 0.08	49.84 ± 0.50	98.1	$4.9^{+0.0}_{-0.0}$	$0.1^{+0.0}_{-0.0}$
HD 178797	6.35 ± 0.05	4201 ± 50	1.67 ± 0.01	−0.63 ± 0.08	4.82 ± 0.50	77.1	$1.4^{+0.1}_{-0.1}$	$2.5^{+0.9}_{-0.6}$
HD 178910	−14.28 ± 0.05	4560 ± 50	2.39 ± 0.00	0.12 ± 0.08	4.38 ± 0.50	76.9	$1.4^{+0.1}_{-0.1}$	$3.4^{+0.6}_{-0.5}$
HD 179396	24.80 ± 0.04	4731 ± 50	2.39 ± 0.01	−0.24 ± 0.08	4.32 ± 0.50	82.7	$1.2^{+0.1}_{-0.1}$	$4.9^{+0.8}_{-0.7}$
HD 180312	−21.94 ± 0.05	4868 ± 50	2.43 ± 0.00	−0.49 ± 0.08	4.25 ± 0.50	73.5	$1.1^{+0.0}_{-0.0}$	$6.3^{+1.3}_{-0.8}$
HD 180475	−45.90 ± 0.08	4129 ± 50	1.50 ± 0.01	−0.85 ± 0.08	5.34 ± 0.50	58.4	$1.1^{+0.1}_{-0.1}$	$5.4^{+1.9}_{-1.5}$
HD 180658	2.97 ± 0.06	4717 ± 50	2.42 ± 0.01	−0.17 ± 0.08	3.99 ± 0.50	72.3	$1.2^{+0.1}_{-0.1}$	$5.2^{+1.2}_{-0.8}$
HD 180682	30.99 ± 0.07	4077 ± 50	1.47 ± 0.01	−1.03 ± 0.08	5.75 ± 0.50	80.1	$0.8^{+0.1}_{-0.0}$	$14.9^{+1.9}_{-3.2}$
HD 181022	−80.39 ± 0.16	3557 ± 50	1.05 ± 0.01	−1.63 ± 0.08	4.68 ± 0.50	108.8	$0.9^{+0.1}_{-0.1}$	$10.0^{+3.4}_{-2.6}$
HD 181069	9.99 ± 0.05	4740 ± 50	2.51 ± 0.00	−0.09 ± 0.08	3.95 ± 0.50	90.0	$1.5^{+0.0}_{-0.0}$	$2.7^{+0.3}_{-0.3}$
HD 181097	−5.60 ± 0.08	4389 ± 50	1.93 ± 0.01	−0.39 ± 0.08	4.50 ± 0.50	69.7	$1.5^{+0.1}_{-0.1}$	$2.5^{+0.6}_{-0.5}$
HD 181597	−13.06 ± 0.04	4612 ± 50	2.30 ± 0.00	−0.35 ± 0.08	3.51 ± 0.50	161.8	$1.5^{+0.1}_{-0.0}$	$2.6^{+0.2}_{-0.3}$
HD 181778	−22.04 ± 0.06	4608 ± 50	2.25 ± 0.01	−0.21 ± 0.08	4.36 ± 0.50	87.6	$2.2^{+0.0}_{-0.1}$	$0.8^{+0.1}_{-0.1}$
HD 181880	0.56 ± 0.08	4200 ± 50	1.68 ± 0.01	−0.56 ± 0.08	4.91 ± 0.50	71.2	$1.6^{+0.1}_{-0.1}$	$1.8^{+0.4}_{-0.3}$
HD 182354	−36.79 ± 0.06	4697 ± 50	2.29 ± 0.01	−0.30 ± 0.08	5.38 ± 0.50	166.5	$2.4^{+0.1}_{-0.1}$	$0.7^{+0.1}_{-0.1}$
HD 182531	−7.34 ± 0.05	4204 ± 50	1.68 ± 0.01	−0.49 ± 0.08	4.94 ± 0.50	71.4	$1.6^{+0.1}_{-0.1}$	$1.8^{+0.4}_{-0.2}$
HD 182692	−8.01 ± 0.04	4762 ± 50	2.54 ± 0.00	0.03 ± 0.08	4.55 ± 0.50	72.8	$1.5^{+0.0}_{-0.0}$	$3.2^{+0.3}_{-0.3}$
HD 182694	−0.87 ± 0.06	5089 ± 50	2.75 ± 0.01	−0.19 ± 0.08	5.30 ± 0.50	187.2	$2.7^{+0.0}_{-0.1}$	$0.5^{+0.1}_{-0.0}$
HD 183124	14.96 ± 0.02	4781 ± 50	2.49 ± 0.00	−0.27 ± 0.08	5.51 ± 0.50	114.3	$1.4^{+0.0}_{-0.0}$	$3.1^{+0.5}_{-0.3}$
HD 185286	−13.70 ± 0.08	4090 ± 50	1.49 ± 0.01	−0.37 ± 0.08	5.98 ± 0.50	135.6	$1.7^{+0.1}_{-0.1}$	$1.9^{+0.5}_{-0.3}$
HD 188537	−18.03 ± 0.15	4776 ± 50	2.02 ± 0.01	−0.24 ± 0.08	10.98 ± 0.50	67.0	$3.3^{+0.1}_{-0.1}$	$0.3^{+0.0}_{-0.0}$
HD 189750	−62.65 ± 0.06	4814 ± 50	2.46 ± 0.01	−0.34 ± 0.08	4.15 ± 0.50	100.8	$1.3^{+0.1}_{-0.1}$	$3.6^{+1.1}_{-0.7}$
HD 226754	18.66 ± 0.10	4184 ± 50	1.74 ± 0.01	−0.12 ± 0.08	5.33 ± 0.50	62.5	$1.3^{+0.1}_{-0.1}$	$4.4^{+1.6}_{-1.1}$

families in a differential way with respect to Arcturus. The chemical composition for the neutron capture elements are shown in Fig. 6, and are derived in absolute terms and not differentially with respect to Arcturus. The elemental abundance ratios were measured in order to assess the Galactic populations to which these stars belong. The first thing to note is that the metallicities, which are tabulated in Table 3, are too high (with $-0.51 <$ [M/H] $< +0.14$ dex) to belong to the Galactic halo, whose peak metallicity is around ~ -1.50 (e.g. Chiba & Beers 2000). Furthermore, the distance distribution, noted in Table 1, indicates that all stars are located within a few kpc of the Sun and are not apart of the Galactic bulge. Thus, these stars are drawn from only the Galactic thick and thin disks. We provide a detailed chemical abundance analysis below to support this claim.

One of the primary ways to determine, in a chemical sense, whether the stars in our sample are drawn from the Galactic disk(s), bulge or halo, is with the ratio of their α-elements to Fe. The α elements are formed during He burning (e.g. Mg, Ti, Si, Ca) and largely dispersed into the interstellar medium through Type II supernovae (SNII) (Matteucci & Recchi 2001). It has been shown by many studies (e.g. Edvardsson et al. 1993; Adibekyan et al. 2012; Feltzing & Chiba 2013; Bensby et al. 2014, and references therein), that the Galactic thick disk and thin disk separate in the α elements, where the thick disk is enhanced in [Mg, Si, Ca, Ti/Fe] compared to the Galactic thin disk at a given metallicity. In Fig. 5, we display the [Mg/Fe] abundance ratio as a function of [Fe/H] for our stars (black circles) compared[1] to representative thick and thin disk stars from (Bensby et al. 2014, open red square) and (Adibekyan et al. 2012, open orange triangles).

For most of the stars in our sample, the [Mg/Fe] abundance ratios are enhanced. This is true for all of the α-elements except Ca where the is a much larger spread. The commonly used [α/Fe] abundance ratio, the average of Mg, Ti, Si, Ca (thus it is ([Mg/Fe] + [Ca/Fe] + [Si/Fe] + [Ti/Fe] / 4)), is also enhanced in most stars. This is consistent with most of the stars observed here belonging to the Galactic disk with a slight (of order ~0.15 dex) enhancement in the α-elements. Fig. 5 clearly rule out the Galactic bulge (which would require the sample to be significantly more α-enriched given their metallicity) and the Galactic halo (given that the stars would need to be significantly more metal-poor).

[1] There may to be systematics between our [X/Fe] abundance scale and those of our comparison samples.

Table 4. Chemical abundances relative to iron for stars in the red giant sample as determined by BACCHUS, differential line-by-line comparison to Arcturus, as described in Section 2.4, for the elements Ca, Mg, Si, Ti, Al, Ba, and Na. Dashes indicate elements for which abundances could not be reliably computed.The catalogue of abundances for neutron capture elements continues in Table 5.

Object	[Mg/Fe]	[Ti/Fe]	[Si/Fe]	[Ca/Fe]	[Al/Fe]	[V/Fe]	[Ni/Fe]
BD 36 3564	0.36 ± 0.09	0.03 ± 0.10	0.27 ± 0.03	−0.04 ± 0.02	0.25 ± 0.02	−0.13 ± 0.03	−0.03 ± 0.06
BD 39 3577	0.25 ± 0.05	−0.17 ± 0.03	0.13 ± 0.03	0.13 ± 0.05	0.17 ± 0.03	−0.29 ± 0.02	−0.02 ± 0.04
BD 42 3150	0.17 ± 0.05	0.09 ± 0.06	0.13 ± 0.03	0.06 ± 0.03	0.22 ± 0.01	−0.02 ± 0.02	0.07 ± 0.03
BD 48 2904	0.12 ± 0.02	0.07 ± 0.04	0.19 ± 0.03	0.06 ± 0.09	0.30 ± 0.03	0.01 ± 0.03	0.06 ± 0.03
BD 48 2955	0.21 ± 0.01	−0.14 ± 0.10	0.25 ± 0.03	−0.09 ± 0.07	0.13 ± 0.04	−0.12 ± 0.07	0.01 ± 0.05
HD 174829	0.14 ± 0.16	0.11 ± 0.03	0.14 ± 0.04	−0.02 ± 0.04	0.20 ± 0.03	−0.10 ± 0.02	−0.07 ± 0.04
HD 175740	–	–	–	–	–	–	–
HD 175884	0.12 ± 0.03	0.10 ± 0.05	0.12 ± 0.02	−0.00 ± 0.04	0.22 ± 0.00	−0.07 ± 0.06	0.07 ± 0.04
HD 178797	0.20 ± 0.03	0.02 ± 0.00	0.22 ± 0.03	−0.05 ± 0.03	0.23 ± 0.07	−0.16 ± 0.03	0.01 ± 0.04
HD 178910	0.18 ± 0.06	0.05 ± 0.07	0.24 ± 0.05	0.11 ± 0.01	0.32 ± 0.05	0.26 ± 0.09	0.29 ± 0.03
HD 179396	0.17 ± 0.01	0.07 ± 0.06	0.17 ± 0.05	0.01 ± 0.04	0.23 ± 0.05	−0.05 ± 0.02	−0.00 ± 0.03
HD 180312	0.19 ± 0.03	0.11 ± 0.05	0.07 ± 0.04	0.06 ± 0.06	0.25 ± 0.05	−0.12 ± 0.02	0.00 ± 0.03
HD 180475	0.20 ± 0.01	0.16 ± 0.05	0.17 ± 0.04	−0.09 ± 0.03	0.16 ± 0.02	−0.24 ± 0.03	−0.03 ± 0.04
HD 180658	0.12 ± 0.01	0.08 ± 0.02	0.08 ± 0.04	0.04 ± 0.05	0.27 ± 0.05	0.02 ± 0.03	0.04 ± 0.04
HD 180682	0.42 ± 0.03	0.12 ± 0.08	0.38 ± 0.03	−0.13 ± 0.04	0.20 ± 0.06	−0.29 ± 0.02	0.07 ± 0.03
HD 181069	0.15 ± 0.06	0.06 ± 0.02	0.13 ± 0.05	0.01 ± 0.01	0.20 ± 0.05	−0.01 ± 0.03	0.08 ± 0.04
HD 181097	0.26 ± 0.02	0.10 ± 0.03	0.14 ± 0.04	0.06 ± 0.06	0.26 ± 0.03	0.02 ± 0.03	0.03 ± 0.03
HD 181597	0.08 ± 0.02	0.11 ± 0.04	0.08 ± 0.02	0.11 ± 0.03	0.22 ± 0.00	−0.02 ± 0.02	0.08 ± 0.03
HD 181778	0.04 ± 0.04	−0.00 ± 0.01	0.05 ± 0.03	0.01 ± 0.02	0.21 ± 0.03	−0.10 ± 0.02	0.06 ± 0.04
HD 181880	0.26 ± 0.08	−0.01 ± 0.03	0.25 ± 0.04	−0.03 ± 0.03	0.27 ± 0.05	−0.07 ± 0.02	0.03 ± 0.04
HD 182354	0.06 ± 0.08	0.04 ± 0.03	0.10 ± 0.02	0.08 ± 0.03	0.13 ± 0.06	−0.10 ± 0.02	−0.03 ± 0.04
HD 182531	0.07 ± 0.03	0.04 ± 0.10	0.09 ± 0.05	−0.03 ± 0.03	0.20 ± 0.06	−0.07 ± 0.10	0.08 ± 0.03
HD 182692	0.09 ± 0.02	0.13 ± 0.03	0.13 ± 0.03	0.11 ± 0.04	0.25 ± 0.05	0.01 ± 0.03	0.07 ± 0.04
HD 182694	0.03 ± 0.03	0.07 ± 0.02	0.06 ± 0.03	0.07 ± 0.02	0.12 ± 0.03	−0.14 ± 0.02	−0.07 ± 0.04
HD 183124	0.18 ± 0.02	0.06 ± 0.04	0.15 ± 0.04	0.09 ± 0.04	0.25 ± 0.04	−0.10 ± 0.02	0.00 ± 0.04
HD 185286	0.19 ± 0.04	−0.14 ± 0.10	0.17 ± 0.04	0.02 ± 0.02	0.23 ± 0.01	0.04 ± 0.09	0.12 ± 0.04
HD 188537	0.27 ± 0.03	0.05 ± 0.07	0.16 ± 0.02	0.08 ± 0.04	0.28 ± 0.10	−0.04 ± 0.03	0.03 ± 0.06
HD 189750	0.13 ± 0.04	0.08 ± 0.02	0.10 ± 0.02	0.06 ± 0.03	0.19 ± 0.05	−0.10 ± 0.02	0.04 ± 0.03
HD 226754	0.25 ± 0.05	−0.10 ± 0.10	0.13 ± 0.04	−0.02 ± 0.00	0.26 ± 0.06	−0.07 ± 0.10	0.05 ± 0.03

In addition, to the α and odd-Z elements we also derived the chemical abundance for several neutron capture elements including Sr, Zr, La, Eu (left panel of Fig 6) as well as Y, Ba, and Nd (right panel of Fig. 6). It is clear from Fig. 6 that the chemical abundance ratio of neutron each neutron capture element is consistent with the Galactic disk population. We do however observe that the Ba of our sample is slightly enhanced while the Y of our sample is slightly reduced relative to the general disk population of Bensby et al. (2014). Nevertheless, we conclude all elemental abundance ratios studied our sample most closely resemble the Galactic disk.

We note that one of the stars (HD 175740) can also be found in the Hypatia catalogue (Hinkel et al. 2014). The chemical abundance ratios in each element are consistent, within the uncertainties (of order ∼0.10–0.15 dex for most elemental abundance ratios in Hypatia and up to ∼0.05 dex here).

3.1.2 Red Clump Stars

Red clump stars, which burn helium in their cores, can be distinguished from hydrogen-shell burning giants asteroseismologically, via their much higher g-mode period spacings (Bedding et al. 2011). The term 'red clump' arises from the fact that such stars can have a very narrow range of luminosities, so that they appear as a clump in the HR diagram (Girardi 2016). This property makes them useful standard candles to which distances can be accurately computed from photometry. Red clump stars have been used to calibrate the *Gaia* survey's parallaxes at long distances (Davies et al. 2017; Hawkins et al. 2017; Ruiz-Dern et al. 2018). *Gaia* DR2 parallaxes have a zero-point offset of ∼ 0.03 mas (Lindegren et al. 2018), and in particular hierarchical models of the ensemble of *Gaia* clump stars can be used to accurately estimate this and thereby improve the accuracy of *Gaia* distances greater than a few kpc (Hawkins et al., in prep.).

From inspection of the power spectra, HD 181069, HD 183124, HD 182354, HD 182692, and HD 180658 are seen to be red clump stars. A power spectrum of the best example of these, HD 183124, together with an échelle diagram used to estimate its g-mode period spacing, is shown in Figure 7. While precise characterization of these stars is beyond the scope of this paper, they are ideal candidates for anchoring models of the mass and metallicity dependence of red clump properties for calibrating *Gaia* and other distance measures.

3.1.3 Long Period Variables

3.2 Main Sequence Stars

For all the main sequence stars in our sample, we inspected light curves and power spectra to determine their variability class. In the following subsections, we will briefly comment on some of the findings. Since main sequence variables are so diverse, and the relevant scientific questions so varied, we have attempted only a very preliminary study of these stars in this paper, leaving detailed analysis to future work.

Our sample includes pulsating stars of spectral type B, A,

Table 5. Chemical abundances relative to iron of neutron capture elements for stars in the red giant sample as determined by BACCHUS, without differential line-by-line comparison to Arcturus, as described in Section 2.4, for the elements Ni, Mn, Co, Eu, La, Zr, and Sr. Dashes indicate elements for which abundances could not be reliably computed.

Object	[Sr/Fe]	[Y/Fe]	[Zr/Fe]	[Ba/Fe]	[La/Fe]	[Eu/Fe]
BD+36 3564	0.34 ± 0.12	−0.27 ± 0.02	0.10 ± 0.02	–	−0.02 ± 0.07	0.25 ± 0.03
BD+39 3577	–	−0.40 ± 0.04	0.13 ± 0.08	0.35 ± 0.10	−0.25 ± 0.02	−0.22 ± 0.04
BD+43 3064	0.25 ± 0.12	−0.14 ± 0.05	0.32 ± 0.04	–	0.15 ± 0.02	0.28 ± 0.06
BD+43 3171	–	−0.31 ± 0.03	0.36 ± 0.07	0.33 ± 0.18	−0.06 ± 0.11	0.21 ± 0.05
BD+43 3213	0.64 ± 0.47	−0.06 ± 0.09	0.49 ± 0.11	–	−0.11 ± 0.05	0.06 ± 0.04
BD+48 2955	–	−0.15 ± 0.05	0.34 ± 0.05	–	0.24 ± 0.05	0.28 ± 0.04
HD 174020	0.37 ± 0.89	−0.19 ± 0.06	–	–	0.02 ± 0.07	0.11 ± 0.04
HD 174829	–	−0.25 ± 0.06	0.08 ± 0.03	–	0.12 ± 0.05	0.15 ± 0.01
HD 175740	–	−0.09 ± 0.07	0.18 ± 0.02	0.30 ± 0.07	0.12 ± 0.01	0.09 ± 0.07
HD 175884	–	−0.21 ± 0.07	0.26 ± 0.02	–	0.14 ± 0.03	0.19 ± 0.02
HD 178797	–	−0.08 ± 0.05	0.23 ± 0.03	0.39 ± 0.22	0.14 ± 0.02	0.26 ± 0.02
HD 178910	–	−0.18 ± 0.05	0.00 ± 0.03	0.25 ± 0.08	−0.13 ± 0.06	−0.02 ± 0.06
HD 179396	–	−0.27 ± 0.07	0.04 ± 0.02	0.31 ± 0.03	0.05 ± 0.03	−0.05 ± 0.03
HD 179959	–	−0.08 ± 0.06	0.14 ± 0.07	–	0.18 ± 0.01	0.16 ± 0.06
HD 180312	–	−0.23 ± 0.05	0.08 ± 0.02	0.37 ± 0.08	0.04 ± 0.07	0.34 ± 0.05
HD 180475	–	−0.25 ± 0.08	0.25 ± 0.03	0.30 ± 0.20	0.18 ± 0.03	0.19 ± 0.07
HD 180658	–	−0.20 ± 0.01	0.16 ± 0.07	0.21 ± 0.09	0.04 ± 0.04	–
HD 180682	–	−0.29 ± 0.04	0.22 ± 0.03	0.19 ± 0.05	−0.03 ± 0.02	0.26 ± 0.03
HD 181022	–	−0.23 ± 0.02	0.36 ± 0.14	0.31 ± 0.23	−0.03 ± 0.21	0.26 ± 0.03
HD 181069	–	−0.11 ± 0.08	0.10 ± 0.03	0.26 ± 0.09	0.02 ± 0.04	0.09 ± 0.03
HD 181097	–	−0.21 ± 0.03	0.23 ± 0.03	–	0.17 ± 0.02	0.28 ± 0.04
HD 181597	–	−0.19 ± 0.08	0.26 ± 0.03	0.28 ± 0.05	0.13 ± 0.01	0.18 ± 0.03
HD 181778	–	−0.13 ± 0.04	0.11 ± 0.03	0.47 ± 0.05	0.08 ± 0.03	0.16 ± 0.01
HD 181880	–	−0.20 ± 0.07	0.33 ± 0.04	–	0.17 ± 0.02	0.32 ± 0.04
HD 182531	0.35 ± 0.14	−0.19 ± 0.07	0.36 ± 0.03	–	0.15 ± 0.03	0.16 ± 0.05
HD 182692	–	−0.21 ± 0.10	0.21 ± 0.03	0.13 ± 0.05	0.06 ± 0.04	0.01 ± 0.05
HD 182694	–	−0.12 ± 0.05	0.16 ± 0.04	–	0.16 ± 0.02	0.16 ± 0.02
HD 183124	–	−0.24 ± 0.03	0.14 ± 0.04	0.25 ± 0.05	0.04 ± 0.06	0.17 ± 0.05
HD 185286	0.30 ± 0.05	−0.19 ± 0.08	0.52 ± 0.05	–	0.12 ± 0.05	0.18 ± 0.03
HD 185351	–	−0.16 ± 0.05	0.29 ± 0.04	0.21 ± 0.09	0.13 ± 0.03	−0.06 ± 0.06
HD 187217	–	−0.37 ± 0.05	0.22 ± 0.04	0.21 ± 0.14	−0.07 ± 0.03	–
HD 188537	–	−0.27 ± 0.09	0.30 ± 0.04	0.24 ± 0.07	0.15 ± 0.10	0.20 ± 0.04
HD 188629	0.34 ± 0.22	−0.04 ± 0.10	0.43 ± 0.01	–	0.06 ± 0.07	0.15 ± 0.03
HD 188875	–	−0.04 ± 0.07	0.30 ± 0.03	–	0.20 ± 0.05	0.19 ± 0.07
HD 226754	0.26 ± 0.13	−0.33 ± 0.04	0.34 ± 0.04	0.43 ± 0.00	−0.05 ± 0.07	0.28 ± 0.07

and F, with their names, properties and variability class listed in Table 1.

Among the hot-star sample are 5 δ Sct stars, which show p-mode pulsation. These oscillation modes have particularly long lifetimes and stable frequencies, making them precise stellar clocks with periods of ∼2 hr. These can be used to search for binarity and to obtain orbital parameters from photometry alone (Shibahashi & Kurtz 2012). We used the phase-modulation method of Murphy et al. (2014) to investigate whether any of these δ Sct stars were binaries. Any phase modulation is converted into a light arrival-time delay, and if a star is a binary, the time delays of each mode should vary in unison. Nearly 350 PM binaries are known in the full *Kepler* dataset (Murphy et al. 2018).

In four of the five targets we found evidence for binarity, while in the fifth (HD 185397) there was some time-delay variation but there was no agreement between different modes so it is not of binary origin. Of the others, HD 175841 and HD 177781 are likely very long-period binaries, with periods far exceeding the Kepler datasets of ∼1470 d. HD 181521 appears to be an eccentric binary with a period of at least 1000 d, but there is only 1 maximum and 1 minimum in the time-delay curve (cf. (Murphy & Shibahashi 2015)), so a unique orbital solution was unobtainable. Finally, HD 186255 is likely a binary with a period of ∼415 d, but there is a slight aperiodicity in the time delays, likely caused by beating between pulsation modes that are not well-separated in the frequency. That, coupled with the fact that this star is on the failed Module 3 and is therefore missing data every 4th quarter (i.e. ∼93 of every 372.5 d), makes the binary classification uncertain. If indeed this is a 415-d binary, the time delays are consistent with a companion of minimum mass ∼0.45 $M_\odot$ in an orbit of moderate eccentricity (∼0.15).

Several stars have a more complex classification than can be adequately noted in Table 1: HD 189684 is listed as an ellipsoidal variable, but also shows evidence for γ Dor variability. HD 185397 and HD 186255 are listed as γ Dor/δ Sct hybrids, but may in fact simply be δ Sct variables with nonlinear combination frequencies, and a detailed frequency analysis will be required to distinguish between these possibilities. HD 184788 shows a combination of two rotational modulation signals with base frequencies: 0.0885 and $0.1966 c/d$. HD 184875 is a γ Dor but also shows evidence for an unknown contaminant. V554 Lyr and V2079 Cyg are both known α^2 CVn variables, which are chemically peculiar stars with strong magnetic fields that show rotational modulation. V2079 Cyg also shows a weak δ Sct signal. The detection of rotational modulation

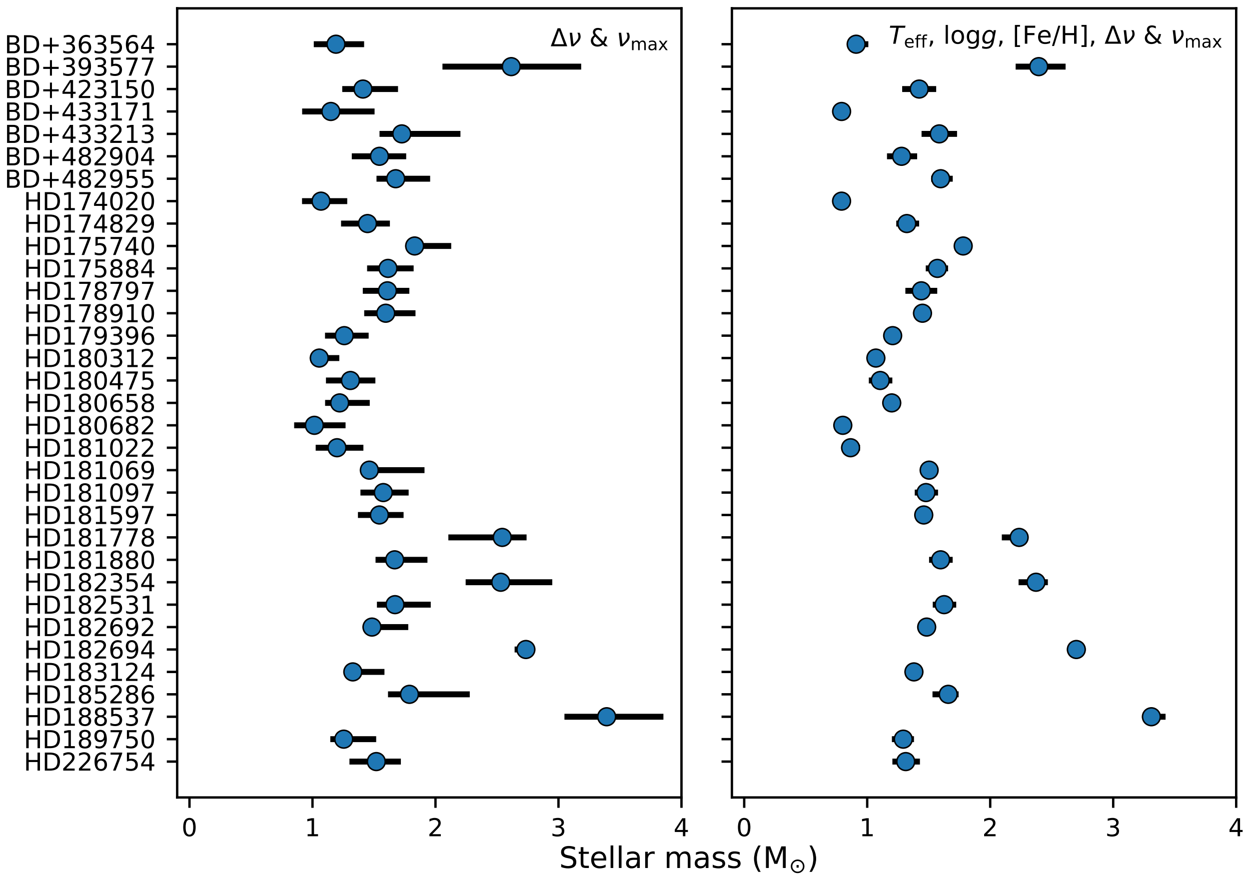

Figure 4. Using asteroseismic constraints (left) and asteroseismic and spectroscopic constraints jointly (right) we infer the masses of each star in the asteroseismic sample of giants.

in the chemically-peculiar HD 175132 suggests its reclassification as an α^2 CVn variable.

There are two stars whose variability we classify as α^2 CVn HD 176582 (B5V) and HD 179395 (B9), but which are not previously known to be chemically-peculiar. have very short periods (1.58 d and 1.83 d respectively) and phase stability throughout the *Kepler* observations. While HD 176582 is listed as an eruptive variable by Davenport (2016), this appears to be a misclassification considering the full *Kepler* smear light curve. Both stars show periods shorter than the shortest 'heartbeat' binaries with tidally-induced pulsations from Thompson et al. (2012). Moreover, the variability periods are short enough that for a binary origin we would expect orbits to be circularized (Debernardi et al. 2000). We suggest that it is likely that these are nevertheless α^2 CVn variables, and that it will be valuable to study these stars spectroscopically for signs of chemical peculiarity.

The coherent g-mode pulsations in samples of B, A, and F stars observed by *Kepler* previously showed these stars to be near-rigid rotators (Kurtz et al. 2014; Saio et al. 2015; Triana et al. 2015; Van Reeth et al. 2015, 2016, 2018; Murphy et al. 2016; Schmid & Aerts 2016; Moravveji et al. 2016; Ouazzani et al. 2017; Pápics et al. 2017; Aerts et al. 2017; Szewczuk & Daszyńska-Daszkiewicz 2018; Aerts et al. 2018a). These studies cover about 70 stars so far. However, the vast majority of intermediate-mass stars observed by Kepler have yet to be subjected to in-depth asteroseismic analyses and modelling of their interior properties. One of the valuable outputs of our current work includes the reduced light curves of several early-B stars, which were only scarcely targeted in the nominal *Kepler* mission. The few that were monitored did not reveal suitable oscillation frequency patterns to achieve a unique mode identification, which is a requirement to perform asteroseismic modelling. The investigation of pulsation modes in high-mass stars using high-quality *Kepler* smear data combined with high-precision spectroscopy to identify the modes (Aerts et al. 2010, Chapter 6) is an exciting prospect for asteroseismology, as the interior physics of these stars are largely unknown, yet they play a pivotal role in stellar and galactic evolution. The in-depth asteroseismic analysis of the smear data for the B stars in this work is beyond the scope of the current paper, as it requires additional ground-based follow-up spectroscopy. Such studies will be the subject of future work.

3.2.1 Hump and Spike Stars

Several stars in the sample show the 'hump-and-spike' morphology in their power spectra (a broad 'hump' of low-amplitude oscillations dominated by one high amplitude coherent oscillation toward the high frequency end of this band): HD 186155 (HR 7495), 14 Cyg (HD 185872, HR 7483), HD 189178 (HR 7628), HD 183362 (HR 7403), and HD 184787. Of these, HD 186155 and 14 Cyg are the third– and sixth–brightest stars on silicon, making these the brightest stars that show this effect. The identification for HD 189178 is tentative, as the spectrum also shows evidence of

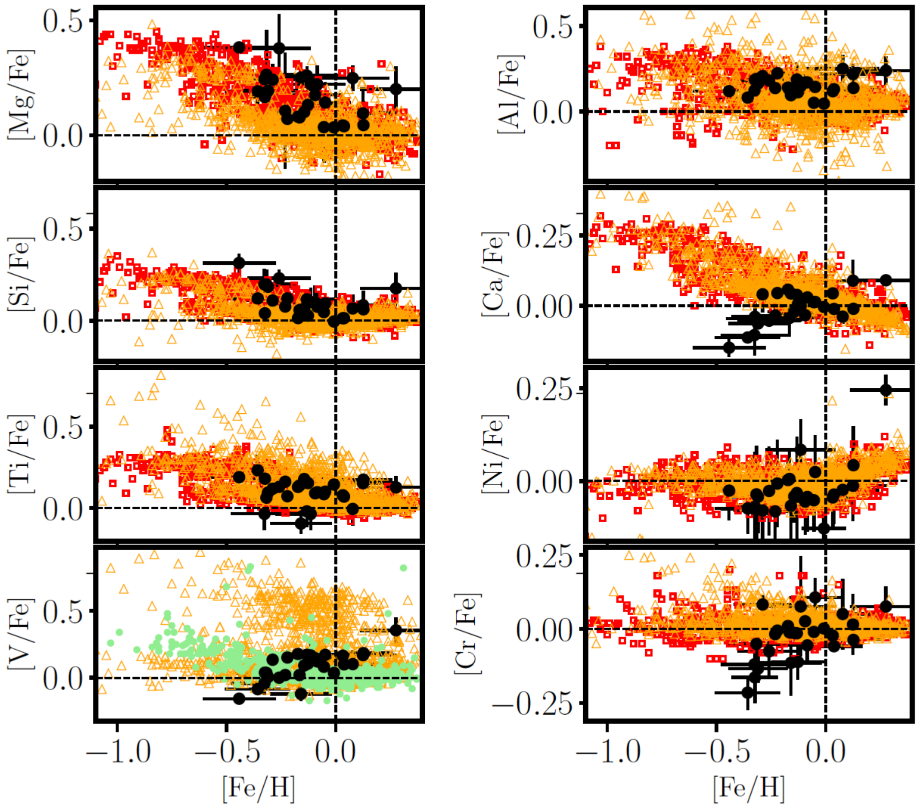

Figure 5. The [Mg/Fe], [Si/Fe], [Ti/Fe], [V/Fe] (left panel) and [Al/Fe], [Ca/Fe], [Ni/Fe], [Cr/Fe] (right panel) abundance ratios as a function of iron for our stars (black circles). We also show a representative sample of Galactic disk stars from Bensby et al. (open red square, 2014), Adibekyan et al. (open orange squares, 2012), Battistini & Bensby (light green circles 2015). These elemental ratios show that the chemical composition of our sample is consistent with the Galactic disk population.

SPB pulsations, and for HD 183362 for γ Dor pulsations, while for HD 184787 there is long term variability consistent with contamination. The other hump-and-spike identifications seem secure. Saio et al. (2018) have recently interpreted the hump-and-spike power spectra as evidence for Rossby modes. The F5 star HD 186155, identified by SIMBAD as having a giant spectral type of F5II-III, is shown by its *Gaia* distance to in fact lie on the main sequence. A detailed study of these stars will be presented by Antoci et al., in prep.

Another star with a hump-and-spike spectrum is Boyajian's Star (KIC 8462852), which shows deep enigmatic dips in brightness (Boyajian et al. 2016), and has faded both throughout the *Kepler* mission (Montet & Simon 2016) and in relation to Harvard photographic plates from 1890 onwards (Schaefer 2016). The dimming, which is chromatic in the manner expected of heterogeneous clouds of circumstellar dust in the line of sight (Davenport et al. 2018; Bodman et al. 2018), has been ascribed to various causes (reviewed in Wright 2018), most notably a cloud of exocomets surrounding the star (e.g. Wyatt et al. 2018). It is unclear whether the explanation of the hump-and-spike phenomenon will shed light on the strange behaviour of Boyajian's Star, but it may be relevant.

3.2.2 Binaries

We detect BD+47 2825 as a new eclipsing binary system, and recover light curves for the previously-known eclipsing binaries HD 186994, V2083 Cyg, and V380 Cyg. The known binary system HD 189684 is newly identified as showing ellipsoidal variability, but does not show evidence of eclipses. We do not attempt detailed analysis of their variability in this paper.

4 OPEN SCIENCE

We believe in open science, and have therefore made all substantive products of this research available to the interested reader. All code used to produce smear light curves is available under a GPL v3 license at `github.com/benjaminpope/keplersmear`. All smear light curves, both including the red giant sample studied in detail in Section 3.1, and main sequence stars as discussed in Sections 3.2 and 3.2.2, can be downloaded from the Mikulski Archive for Space Telescopes (MAST) as a High-Level Science Product. TRES spectra will be made available from the ExoFOP-TESS website, and all asteroseismic parameters and derived stellar parameters for the red giants in Section 3.1 are provided in an online-only table as Supplementary Material to this paper.

All smear light curves in this paper, as well as the LaTeX source code used to produce this document, can be found at `github.com/benjaminpope/smearcampaign`.

5 CONCLUSIONS

The *Kepler* Smear Campaign establishes a legacy sample of 102 very bright stars, with *Kepler* light curves that in almost all cases re-

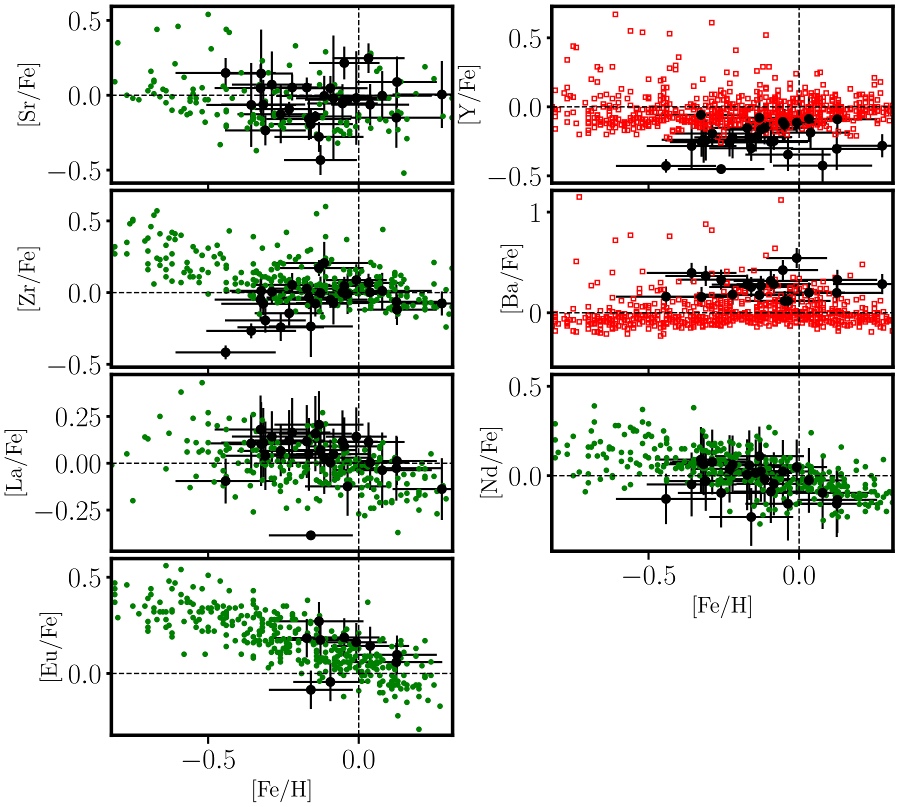

Figure 6. The [Mg/Fe], [Si/Fe], [Ti/Fe], [V/Fe] (left panel) and [Al/Fe], [Ca/Fe], [Ni/Fe], [Cr/Fe] (right panel) abundance ratios as a function of iron for our stars (black circles). We also show a representative sample of Galactic disk stars from Bensby et al. (open red square, 2014), Battistini & Bensby (green circles 2016). These elemental ratios give a representive example of the chemical composition of our sample and show they are consistent with the Galactic disk population.

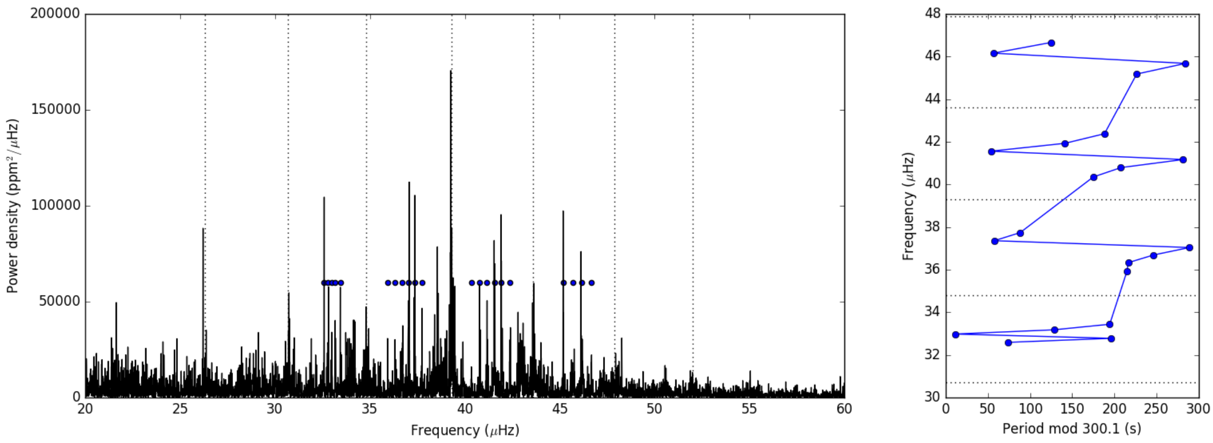

Figure 7. Power spectrum (left) and échelle diagram (right) of the solar-like oscillations of the red clump star HD 183124. The modes in the power spectrum used for the échelle diagram are highlighted with blue dots. In the échelle diagram we see the characteristic pattern of 'bumped' modes from avoided crossings between the comb of p-modes and g-mode oscillations with a period spacing of $\Delta\Pi = 300.1$ s.

veal astrophysically interesting variability. The virtue of these bright stars is that they can be studied with interferometry, and more easily with spectroscopy than fainter targets, permitting especially detailed characterization. We have therefore obtained detailed abundances of a subset of the red giants in this sample, particularly with a view to determining their provenance in the Galactic thick and thin disk populations. The science that can be done both with this sample and with this method are, however, considerably broader: while we have not attempted it in this paper, a compelling next step is to use interferometric diameter measurements and to further constrain the red giant parameters, and compare these to the constraints from *Gaia*. Any tension between these measurements will help test and refine the asteroseismic scaling relations, and better models will propagate through to smaller systematic uncertainties in large samples of stars too faint for interferometry. Further improvements will be revealed by the detailed modelling of individual oscillation frequencies in these giants to infer interior structure such as convective overshoot, which is at the time of writing an active topic of research. For the lower-frequency M giants classed as LPVs in this paper, extending the systematics correction and quarter-stitching algorithms to more robustly correct their light curves without removing real signal will allow similar asteroseismic analysis, for a sample of stars that are much less well understood than their higher-frequency counterparts.

The *Kepler* Smear Campaign has another natural extension: while many saturated stars in *K2* have now been observed with 'halo' apertures including their unsaturated pixels, many were not, either because they were fainter than the typical $Kp \lesssim 6.5$ limit, or because in Campaigns 0-3 and 5 no such apertures were selected. There is therefore the potential for a *K2* Smear Campaign to complete the *K2* sample down to fainter magnitudes, complementing the very brightest stars studied with halo photometry.

ACKNOWLEDGEMENTS

This work was performed in part under contract with the Jet Propulsion Laboratory (JPL) funded by NASA through the Sagan Fellowship Program executed by the NASA Exoplanet Science Institute. B.P. also acknowledges support from Balliol College and the Clarendon Fund. D.H. acknowledges support by the Australian Research Council's Discovery Projects funding scheme (project number DE140101364) and support by the NASA Grant NNX14AB92G issued through the *Kepler* Participating Scientist Program. DWL acknowledges partial support from the Kepler Extended Mission under NASA Cooperative Agreement NNX13AB58A with the Smithsonian Astrophysical Observatory. The research leading to these results has received funding from the European Research Council (ERC) under the European Union's Horizon 2020 research and innovation programme (grant agreement No670519: MAMSIE).

BP acknowledges being on the traditional territory of the Lenape Nations and recognizes that Manhattan continues to be the home to many Algonkian peoples. We give blessings and thanks to the Lenape people and Lenape Nations in recognition that we are carrying out this work on their indigenous homelands. We would like to acknowledge the Gadigal Clan of the Eora Nation as the traditional owners of the land on which the University of Sydney is built and on which some of this work was carried out, and pay their respects to their knowledge, and their elders past, present and future.

This work has made use of data from the European Space Agency (ESA) mission *Gaia* (`https://www.cosmos.esa.int/gaia`), processed by the *Gaia* Data Processing and Analysis Consortium (DPAC, `https://www.cosmos.esa.int/web/gaia/dpac/consortium`). Funding for the DPAC has been provided by national institutions, in particular the institutions participating in the *Gaia* Multilateral Agreement. This work has in particular made use of the `gaia-kepler.fun` crossmatch database created by Megan Bedell.

This research made use of NASA's Astrophysics Data System; the SIMBAD database, operated at CDS, Strasbourg, France; the IPython package (Pérez & Granger 2007); SciPy (Jones et al. 2001); and Astropy, a community-developed core Python package for Astronomy (Collaboration et al. 2018). Some of the data presented in this paper were obtained from the Mikulski Archive for Space Telescopes (MAST). STScI is operated by the Association of Universities for Research in Astronomy, Inc., under NASA contract NAS5-26555. Support for MAST for non-HST data is provided by the NASA Office of Space Science via grant NNX13AC07G and by other grants and contracts. We acknowledge the support of the Group of Eight universities and the German Academic Exchange Service through the Go8 Australia-Germany Joint Research Co-operation Scheme.

REFERENCES

Adibekyan V. Z., Sousa S. G., Santos N. C., Delgado Mena E., González Hernández J. I., Israelian G., Mayor M., Khachatryan G., 2012, A&A, 545, A32
Aerts C., Christensen-Dalsgaard J., Kurtz D. W., 2010, Asteroseismology
Aerts C., Van Reeth T., Tkachenko A., 2017, ApJ, 847, L7
Aerts C., Mathis S., Rogers T., 2018a, preprint, (arXiv:1809.07779)
Aerts C., et al., 2018b, MNRAS, 476, 1234
Aigrain S., Parviainen H., Pope B. J. S., 2016, MNRAS, 459, 2408
Alvarez R., Plez B., 1998, A&A, 330, 1109
Ambikasaran S., Foreman-Mackey D., Greengard L., Hogg D. W., O'Neil M., 2015, IEEE Transactions on Pattern Analysis and Machine Intelligence, 38
Asplund M., Grevesse N., Sauval A. J., 2005, in Barnes III T. G., Bash F. N., eds, Astronomical Society of the Pacific Conference Series Vol. 336, Cosmic Abundances as Records of Stellar Evolution and Nucleosynthesis. p. 25
Bailer-Jones C. A. L., Rybizki J., Fouesneau M., Mantelet G., Andrae R., 2018, preprint, (arXiv:1804.10121)
Battistini C., Bensby T., 2015, A&A, 577, A9
Battistini C., Bensby T., 2016, A&A, 586, A49
Beck P. G., et al., 2011, Science, 332, 205
Beck P. G., et al., 2012, Nature, 481, 55
Bedding T. R., et al., 2011, Nature, 471, 608
Belkacem K., Goupil M. J., Dupret M. A., Samadi R., Baudin F., Noels A., Mosser B., 2011, A&A, 530, A142
Bensby T., Feltzing S., Oey M. S., 2014, A&A, 562, A71
Blanco-Cuaresma S., Soubiran C., Jofré P., Heiter U., 2014, A&A, 566, A98
Bodman E., Wright J., Boyajian T., Ellis T., 2018, preprint, (arXiv:1806.08842)
Boyajian T. S., et al., 2016, MNRAS, 457, 3988
Brown T. M., Gilliland R. L., Noyes R. W., Ramsey L. W., 1991, ApJ, 368, 599
Brown T. M., Latham D. W., Everett M. E., Esquerdo G. A., 2011, AJ, 142, 112
Buchhave L. A., et al., 2012, Nature, 486, 375
Campante T. L., et al., 2015, ApJ, 799, 170
Casagrande L., et al., 2014, MNRAS, 439, 2060
Casagrande L., et al., 2016, MNRAS, 455, 987
Chaplin W. J., Miglio A., 2013, ARA&A, 51, 353
Chaplin W. J., et al., 2010, ApJ, 713, L169
Chiba M., Beers T. C., 2000, AJ, 119, 2843
Christiansen J. L., et al., 2012, PASP, 124, 1279
Collaboration T. A., et al., 2018, The Astronomical Journal, 156, 123
Creevey O. L., et al., 2013, MNRAS, 431, 2419
Creevey O. L., et al., 2015, A&A, 575, A26
Davenport J. R. A., 2016, ApJ, 829, 23
Davenport J. R. A., et al., 2018, ApJ, 853, 130
Davies G. R., Miglio A., 2016, Astronomische Nachrichten, 337, 774
Davies G. R., et al., 2017, A&A, 598, L4
Debernardi Y., Mermilliod J.-C., Carquillat J.-M., Ginestet N., 2000, A&A, 354, 881
Edvardsson B., Andersen J., Gustafsson B., Lambert D. L., Nissen P. E., Tomkin J., 1993, A&A, 275, 101

Farr W. M., et al., 2018, preprint, (arXiv:1802.09812)
Feltzing S., Chiba M., 2013, New Astron. Rev., 57, 80
Gaia Collaboration et al., 2016, A&A, 595, A1
Gaia Collaboration Brown A. G. A., Vallenari A., Prusti T., de Bruijne J. H. J., Babusiaux C., Bailer-Jones C. A. L., 2018, preprint, (arXiv:1804.09365)
García R. A., et al., 2011, MNRAS, 414, L6
Gilliland R. L., et al., 2010, PASP, 122, 131
Girardi L., 2016, ARA&A, 54, 95
Gustafsson B., Edvardsson B., Eriksson K., Jørgensen U. G., Nordlund Å., Plez B., 2008, A&A, 486, 951
Harvey J., 1985, in Rolfe E., Battrick B., eds, ESA Special Publication Vol. 235, Future Missions in Solar, Heliospheric & Space Plasma Physics.
Hawkins K., et al., 2016a, A&A, 592, A70
Hawkins K., et al., 2016b, A&A, 592, A70
Hawkins K., Masseron T., Jofré P., Gilmore G., Elsworth Y., Hekker S., 2016c, A&A, 594, A43
Hawkins K., Leistedt B., Bovy J., Hogg D. W., 2017, MNRAS, 471, 722
Heiter U., Jofré P., Gustafsson B., Korn A. J., Soubiran C., Thévenin F., 2015, A&A, 582, A49
Hidalgo S. L., et al., 2018, ApJ, 856, 125
Hinkel N. R., Timmes F. X., Young P. A., Pagano M. D., Turnbull M. C., 2014, AJ, 148, 54
Hjørringgaard J. G., Silva Aguirre V., White T. R., Huber D., Pope B. J. S., Casagrande L., Justesen A. B., Christensen-Dalsgaard J., 2017, MNRAS, 464, 3713
Howell S. B., et al., 2014, PASP, 126, 398
Huber D., et al., 2011, ApJ, 743, 143
Huber D., et al., 2012, ApJ, 760, 32
Huber D., et al., 2013, ApJ, 767, 127
Jenkins J. M., et al., 2010, ApJ, 713, L87
Jofré P., 2016, Astronomische Nachrichten, 337, 859
Jofré P., et al., 2014, A&A, 564, A133
Jofré P., et al., 2015, A&A, 582, A81
Jofré P., et al., 2017, A&A, 601, A38
Jones E., Oliphant T., Peterson P., Others 2001, SciPy: Open source scientific tools for Python, http://www.scipy.org/
Kallinger T., et al., 2014, A&A, 570, A41
Kjeldsen H., Bedding T. R., 1995, A&A, 293, 87
Koch D. G., et al., 2010, ApJ, 713, L79
Kolodziejczak J., Caldwell D., 2011, Technical Report 20120003045, Science from Kepler Collateral Data: 150 ksec/year from 13 Million Stars?, http://ntrs.nasa.gov/archive/nasa/casi.ntrs.nasa.gov/20120003045.pdf. NASA Marshall Space Flight Centre, http://ntrs.nasa.gov/archive/nasa/casi.ntrs.nasa.gov/20120003045.pdf
Kurtz D. W., Saio H., Takata M., Shibahashi H., Murphy S. J., Sekii T., 2014, MNRAS, 444, 102
Lindegren L., et al., 2018, preprint, (arXiv:1804.09366)
Lomb N. R., 1976, Ap&SS, 39, 447
Lund M. N., et al., 2016, preprint, (arXiv:1612.00436)
Masseron T., et al., 2014, A&A, 571, A47
Masseron T., Merle T., Hawkins K., 2016, BACCHUS: Brussels Automatic Code for Characterizing High accUracy Spectra, Astrophysics Source Code Library (ascl:1605.004), doi:10.20356/C4TG6R
Matteucci F., Recchi S., 2001, ApJ, 558, 351
Montet B. T., Simon J. D., 2016, ApJ, 830, L39
Moravveji E., Townsend R. H. D., Aerts C., Mathis S., 2016, ApJ, 823, 130
Mosser B., et al., 2012a, A&A, 540, A143
Mosser B., et al., 2012b, A&A, 548, A10
Mosser B., et al., 2014, A&A, 572, L5
Murphy S. J., Shibahashi H., 2015, MNRAS, 450, 4475
Murphy S. J., Bedding T. R., Shibahashi H., Kurtz D. W., Kjeldsen H., 2014, MNRAS, 441, 2515
Murphy S. J., Fossati L., Bedding T. R., Saio H., Kurtz D. W., Grassitelli L., Wang E. S., 2016, MNRAS, 459, 1201
Murphy S. J., Moe M., Kurtz D. W., Bedding T. R., Shibahashi H., Boffin H. M. J., 2018, MNRAS, 474, 4322
Ouazzani R.-M., Salmon S. J. A. J., Antoci V., Bedding T. R., Murphy S. J., Roxburgh I. W., 2017, MNRAS, 465, 2294
Pápics P. I., et al., 2017, A&A, 598, A74
Pérez F., Granger B. E., 2007, Computing in Science and Engineering, 9, 21
Petigura E. A., Marcy G. W., 2012, PASP, 124, 1073
Pinsonneault M. H., et al., 2014, ApJS, 215, 19
Plez B., 2012, Turbospectrum: Code for spectral synthesis, Astrophysics Source Code Library (ascl:1205.004)
Pope B. J. S., et al., 2016, MNRAS, 455, L36
Ruiz-Dern L., Babusiaux C., Arenou F., Turon C., Lallement R., 2018, A&A, 609, A116
Saio H., Kurtz D. W., Takata M., Shibahashi H., Murphy S. J., Sekii T., Bedding T. R., 2015, MNRAS, 447, 3264
Saio H., Kurtz D. W., Murphy S. J., Antoci V. L., Lee U., 2018, MNRAS, 474, 2774
Scargle J. D., 1982, ApJ, 263, 835
Schaefer B. E., 2016, ApJ, 822, L34
Schmid V. S., Aerts C., 2016, A&A, 592, A116
Serenelli A., et al., 2017, ApJS, 233, 23
Sharma S., Stello D., Bland-Hawthorn J., Huber D., Bedding T. R., 2016, ApJ, 822, 15
Shibahashi H., Kurtz D. W., 2012, MNRAS, 422, 738
Silva Aguirre V., et al., 2013, ApJ, 769, 141
Silva Aguirre V., et al., 2015a, MNRAS, 452, 2127
Silva Aguirre V., et al., 2015b, MNRAS, 452, 2127
Silva Aguirre V., et al., 2016, preprint, (arXiv:1611.08776)
Silva Aguirre V., et al., 2017, ApJ, 835, 173
Smith J. C., et al., 2012, PASP, 124, 1000
Stello D., et al., 2016, ApJ, 832, 133
Stumpe M. C., et al., 2012, PASP, 124, 985
Szewczuk W., Daszyńska-Daszkiewicz J., 2018, MNRAS, 478, 2243
Thompson S. E., et al., 2012, ApJ, 753, 86
Triana S. A., Moravveji E., Pápics P. I., Aerts C., Kawaler S. D., Christensen-Dalsgaard J., 2015, ApJ, 810, 16
Twicken J. D., Chandrasekaran H., Jenkins J. M., Gunter J. P., Girouard F., Klaus T. C., 2010, in Software and Cyberinfrastructure for Astronomy. p. 77401U, doi:10.1117/12.856798
Van Eylen V., Agentoft C., Lundkvist M. S., Kjeldsen H., Owen J. E., Fulton B. J., Petigura E., Snellen I., 2018, MNRAS, 479, 4786
Van Reeth T., et al., 2015, ApJS, 218, 27
Van Reeth T., Tkachenko A., Aerts C., 2016, A&A, 593, A120
Van Reeth T., et al., 2018, preprint, (arXiv:1806.03586)
Viani L. S., Basu S., Chaplin W. J., Davies G. R., Elsworth Y., 2017, ApJ, 843, 11
White T. R., et al., 2011, ApJ, 742, L3
White T. R., et al., 2013, MNRAS, 433, 1262
White T. R., et al., 2015, in European Physical Journal Web of Conferences. p. 06068, doi:10.1051/epjconf/201510106068
White T. R., et al., 2017, MNRAS, 471, 2882
Wright J. T., 2018, Research Notes of the American Astronomical Society, 2, 16
Wyatt M. C., van Lieshout R., Kennedy G. M., Boyajian T. S., 2018, MNRAS, 473, 5286
van Leeuwen F., 2007, A&A, 474, 653

This paper has been typeset from a TEX/LATEX file prepared by the author.